

# Detecting and isolating false data injection attacks on electric vehicles of smart grids using distributed functional observers

Thanh Ngoc Pham  | Amanullah Maung Than Oo | Hieu Trinh 

School of Engineering, Deakin University, Geelong, Victoria, Australia

## Correspondence

Thanh Ngoc Pham, School of Engineering, Deakin University, Warrnambool, Geelong, Victoria 3220, Australia.  
Email: thanh.pham@deakin.edu.au

## Abstract

This paper considers the problem of false data injection attacks (FDIAs) on load frequency control of interconnected smart grids (ISGs) with delayed electric vehicles (EVs) and renewable energies. By intruding incorrect information, unauthorised users can corrupt the system information leading to degradation in the performance and disruptions of ISGs. In this paper, a model of ISGs subject to FDIAs in aggregator of EVs and power plants is first presented. This mathematical representation comprises dynamic interactions of power plants, delayed EVs, renewable energies and FDIAs on both system states and outputs. Based on recent advanced techniques on functional observers and matrix inequalities for time-delay systems, then a new distributed functional observers based scheme is developed to realise the tasks of detecting and isolating FDIAs. Also, an effective procedure presented in tractable linear matrix inequalities build with an optimisation process for the synthesis of the detector. The proposed detector is distributed, of reduced order, avoids the risk of centralised malicious incidents, therefore easy for implementation and monitoring tasks. The stability of ISGs and contribution of EVs subject to FDIAs are also discussed. Comprehensive simulations are given to demonstrate the effectiveness of our proposed method by using three-area ISGs.

## 1 | INTRODUCTION

### 1.1 | Background and motivations

Load frequency control (LFC) is essential in the effective operation of ISGs [1]. Because of variations in load demands, the system frequencies and interchange powers fluctuate from their planned operating points [2]. By taking appropriate control measures, LFC can rebuild the stability of ISGs and preserve the frequencies and interchange powers at the preferred values [3]. In recent years, significant research attention has been focused on the efficient operation of ISGs subjects to cyber-attacks (please refer to survey papers on cyber security of power grids [4], smart grids [5], security control of industrial cyber physical systems [6] and false data injection attack (FDIAs) against cyber-physical power systems [7]. Due to the unexpected actions of unauthorised users that violate or illegally acquire, modify and disrupt information of communication networks [5], ISGs are vulnerable to catastrophic disruptions, disclosure of sensitive information and frauds [8]. In [9], the control action provided by dis-

tributed energy resources (DERs) was corrupted by attacks. The authors in [10] considered a microgrid with deception attacks. In [11], time delay attacks on LFC of ISGs were addressed.

As a communication network-based component of ISGs, LFC of ISGs is managed by supervision control and data acquisition systems [2]. Critical information for control is transferred within the power network through open communication systems [12]. LFC is the interface between intelligent cyberspace and physical facilities [13]. Because it is highly dependent on the wide utilization of communication networks, LFC is inevitably facing threats created by attackers aiming to cause service outages and infrastructural damages [14]. The approach is to intrude security threats (FDIAs) to interrupt the information transferring within the ISGs, modify the system data and results leading to serious degradations in system stability and performance of LFC [15]. LFC requires reliable information of the system frequencies, interchange power deviations and their area control error to determine the correct amount of power flow within the ISGs. In [16], the authors showed that hackers potentially can destroy the system's stability by injecting false

This is an open access article under the terms of the [Creative Commons Attribution](https://creativecommons.org/licenses/by/4.0/) License, which permits use, distribution and reproduction in any medium, provided the original work is properly cited.

© 2020 The Authors. *IET Generation, Transmission & Distribution* published by John Wiley & Sons Ltd on behalf of The Institution of Engineering and Technology

and disruptive information into the system. This will lead to incorrect control input signals and hence degrading the system performance and stability. Therefore, it is important to consider the problem of FDIAs in the application of LFC of ISGs and develop efficient regimes to detect and isolate the attacks happen within the systems.

With the purpose of lowering greenhouse emission and noise pollution, integration of REs and EVs have received great research attention in recent literature [3]. REs can provide additional powers without using natural fuels whereas in [17], the deployment of EVs can improve the reliability and flexibility of ISGs. In [18], reserved powers of EVs also support the power plants in the frequency regulation effectively. Due to the powers of REs depend on natural features such as weather and wind speeds, it is unexpectedly intermittent leading to high fluctuation of system frequencies, hence, a bounded control technique was developed for ISGs with REs and energy storages in [19]. To achieve an effective LFC operation of ISGs, the adverse impact of REs intermittent needs to be eliminated for any control and monitoring tasks such fault detection and isolation. With respect to the use of widespread EVs, in order to participate into LFC, an aggregator (master control) and networked or wide-area communication systems comprising power line communications, general packet radio services, internet, Bluetooth and wireless connections is required [3]. Via network communications, the aggregator collects real time information and re-allocate requested power commands to determine charged/discharged power of connected EVs [20]. One important issue of EVs integration is the existence of time delay due to sudden congestion of communication channels, drop-out and disordering of data packets. In [17, 18, 20], networked time delays related to the integration of EVs were considered in the LFC of smart grids. In fact, communication delays can downgrade or even cause to instability of system dynamic performance, hence robust control laws were introduced for ISGs [12], isolated SGs with EVs [17], ISGs with energy storages [19], ISGs with EVs [20], and microgrids [21]. In these works, stability conditions were derived according to Lyapunov theory and techniques based on matrix inequalities to ensure the stability of the closed-loop systems. By employing high complex communication infrastructures, the operation of EVs aggregator faces to the risks of being vulnerable to FDIAs. Indeed, this issue is similar to the problem happened in LFC central facility, deceptive information is potentially and illegally imposed into the transaction between the aggregator and connected EVs. Thus, unauthorised attackers can deteriorate the performance and stability of ISGs and the EVs system.

One of the key functions that smart grid has pledged to perform is to offer a power to fulfil electricity needs with friendly environmentally source of energy while retaining a satisfactory level of adequacy and security that conventional power systems promise [22]. It is therefore important to develop an adequate approach to detect FDIAs in the LFC of the ISGs incorporated friendly sources such REs and EVs and distinguish the FDIAs happened into LFC and the one links to EVs. This is the main motivation of this paper.

## 1.2 | Related works

A novel detection method for LFC based on multilayer perceptron (MLP) classifier was proposed in [14]. For detection purpose, samples of frequency or area control error (ACE) were collected under both normal and compromised circumstances. MLP classifier was applied to map an optimal function between normal and attacked signals. In this method, quantities of training samples are important to the training, testing of MLP based detector. In [15], the authors introduced a model-based fault detection method using real-time load forecast and simulated measurements obtained from equations that govern the functioning of underlying physical systems. In [16], an online attacks detection framework was presented. In this framework, a dynamic watermarking technique was used as the core algorithm to detect tampered information. A detection scheme based on recurrent neural networks for cyber-attacks on DC microgrid was proposed in [23]. In [24], the authors used a full-order observer (FUO)-based method for a delay-free power grid with FDIAs. In [25], a robust detection filter was derived to identify faults on LFC of delay-free power systems. In this work, a FUO was used to estimate the state vector and a residual generator was obtained based on the error between the system state vector and the estimation to determine the existence of faults. In [26], an unknown input FUO-based detection method was deployed for the LFC of delay-free power systems consisting of thermal plants and load demand changes. In [27], the authors used a stochastic estimator based on the observer proposed in [26] to build a fault detector. In [26, 27], residual generators were designed based on the error between the system state vector and its estimated state vector to trigger an alarm. These proposed techniques [25–27] are interesting and effective for detecting FDIAs. However, the structure of these observers used to build the detectors requires current or last updated information of load demand changes. In practice, it is challenging for ISGs to store and update information of REs for monitoring assignments frequently. In [28], a robust detection technique based on unknown input FUO was derived to detect controller and sensor faults of power plant separately without any need of accessing information of load disturbances. In [29], a centralised FUO based detector for actuator and sensing faults were derived. However, the main problem is that the residual generators in the above references was fundamentally founded by the establishment of FUOs [25], unknown input FUOs [24, 26, 28, 29], stochastic estimator based FUOs [27] with centralised architecture, thus resulted in large size of detector, high cost of computation and complexity of implementation. It is highlighted that these detection methods were proposed for delay-free interconnected power systems only. Moreover, the integration of delayed EVs and the issue of FDIAs on EVs were not considered in any of the above-mentioned works. On the other hand, in the previous studies for EVs (see [17, 18, 20] and the references therein), the problem of isolating and detecting of faults was not considered.

In the light of observer developments, FOs have much more advantages than state observers considered in [24–29]. Indeed,

FOs estimate linear functions of the state vector without estimating all the individual states and so minimize the order of observer (size and weight) and reduce complexity of the designed observers [30]. The significance of this is that design of observer-based detection can now be implemented by using a minimum-order FO leading to the reduction of the cost, weight, volume of engineered systems and simplify their maintenance and installation. Motivated by the benefits of FOs, the authors in [31] introduced a FO-based detection method for a delay-free system. In this work, Lyapunov theory was used to ensure the stability of the estimation error between the function of state vector and its estimation. An improved detection regime based on linear matrix inequalities (LMIs) and Lyapunov theory was proposed for a time-delay system with faulty system dynamics [32]. In these algorithms, the fault diagnosis works use centralized architecture and require to centrally gather and the information of measurements as well as linear function of states from all the remote subsystems, hence leading to the difficulty of practical constraints on the limitation of computational workload and communication bandwidth. To overcome these challenges, a detection based on DFOs infrastructure was derived [33] to identify the actuator's faults which are converted into the model system's state vector. In this work, the Winger based inequality and Lyapunov theory were utilised to synthesis the detector's parameters. However, the implementation of the detector required all instant measured output and hence, the performance of detector is unable to be achieved for ISGs where the FDIAs occur in the process of computing area error control signal.

### 1.3 | Contributions and organisation of the paper

The contributions of this paper are underlined as follows:

- i In this paper, we emphasis on the problem of FDIAs for the LFC operation of ISGs and a proposal of deriving a new method to detect and differentiate the occurrence of each attack. To achieve our objective, we first propose a new model of ISGs incorporating FDIAs, aggregated delay EVs and REs.
- ii A new state space model of ISGs encompassing the dynamic interactions of multiple FDIAs on both system states and outputs, communication time delays, EVs and REs is first derived.
- iii In the next stage, we introduce a new DFO-based detection and isolation schemes to detect and isolate each FDIA. The proposed scheme is derived based on some advanced developments of FOs, novel of Lyapunov stability for time-delay systems and residual generators-based fault detection.
- iv The proposed DFOs detector has the advantages of being less order (small size) comparing to conventional state observer-based detectors. It also handles the existence of time delays, be insensitive to neighbouring FDIAs and the excursion of REs. In addition, the detectors are made of distributed structure, hence, prevented from malicious incidents happened in facility of centralised architecture.

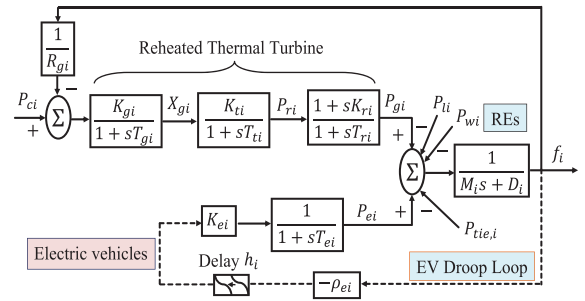


FIGURE 1 A block diagram of transfer functions of an ISG with EVs

- v To synthesis the detector's gains, we derive an effective procedure in tractable LMI, linear computations and an optimisation process, which can be easily solved by efficient computational robust control tool in MATLAB with flexible programming codes.

Finally, for demonstrating the effectiveness of our method, simulations are conducted with a three-area ISGs comprising reheated thermal plants, delayed EVs and REs. We also consider the stability of time delay ISGs and discuss on EVs contribution into frequency services under abnormal performance caused by FDIAs.

The remaining of this paper is outlined as follows: Section 2 introduces a state space model of an ISG with FDIAs, EVs and REs. The DFO-based detection and isolation method with schematic of implementation and a procedure to obtain the detector's parameters are derived in Sections 3 and 4. The effectiveness of our proposed methodology is validated in Section 5. Finally, Section 6 concludes the paper.

## 2 | SYSTEM DESCRIPTION AND PROBLEM STATEMENT

Figure 1 represents a block diagram of transfer functions of an ISG with reheated thermal plants, aggregation of EVs, REs and communication time delays,  $b_i$ ,  $i = 1, \dots, N$ . Due to sudden changes in load demands,  $P_{li}(t)$ , and interruption of REs,  $P_{wi}(t)$ , the system frequencies and interchange powers deviate far from the desirable operating points. To tackle this issue, the local control centre sends a power request command,  $P_{ci}(t)$ , to adjust the output power of thermal power plant. The description of reheated power plant at local power Area- $i^{th}$  depicted in Figure 1 is [20]

$$\begin{aligned}
 \dot{P}_{gi}(t) &= -\frac{1}{T_{ri}}P_{gi}(t) + \frac{K_{ri}K_{ti}}{T_{ti}T_{ri}}X_{gi}(t) + \frac{T_{ti} - K_{ri}}{T_{ti}T_{ri}}P_{ri}(t), \\
 \dot{P}_{ri}(t) &= -\frac{1}{T_{ti}}P_{ri}(t) + \frac{K_{ti}}{T_{ti}}X_{gi}(t), \\
 \dot{X}_{gi}(t) &= -\frac{1}{T_{gi}}X_{gi}(t) + \frac{K_{gi}}{T_{gi}}(P_{ci}(t) - \frac{1}{R_{gi}}f_i(t)), \\
 \dot{f}_i(t) &= -\frac{D_i}{M_i}f_i(t) + \frac{1}{M_i}(P_{gi}(t) + P_{ci}(t) - P_{tie,i}(t)) \\
 &\quad - \frac{1}{M_i}(P_{li}(t) + P_{wi}(t)).
 \end{aligned} \tag{1}$$

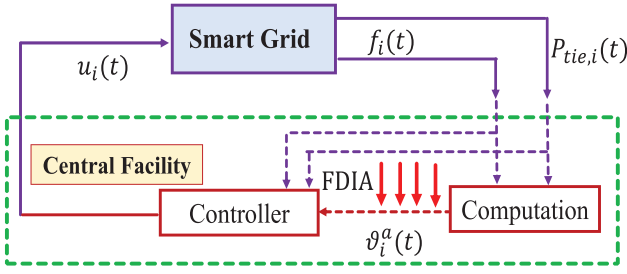


FIGURE 2 Block diagram of FDIA at computation of local Area- $i^{\text{th}}$

The operation of LFC requires the knowledge of area control errors,  $ACE_i(t)$ ,  $i = 1, \dots, N$ , to ensure small steady-state values of system frequency deviation,  $f_i(t)$ , and interchange power (power tie-line) deviation,  $P_{tie,i}(t)$ , when the system subjects to power disturbances. These values are computed according to  $f_i(t)$  and  $P_{tie,i}(t)$  with a frequency bias constant,  $b_i$ , as follows [20]

$$ACE_i(t) = P_{tie,i}(t) + b_i f_i(t), \quad i = 1, \dots, N. \quad (2)$$

By using area control error,  $ACE_i(t)$ , and its integral value,  $\vartheta_i(t) = \int ACE_i(t) dt$ , the control facility of power Area- $i^{\text{th}}$  computes the local power request command,  $P_{ci}(t)$ , as follows [12]

$$P_{ci}(t) = K_{pi} ACE_i(t) + K_{fi} \vartheta_i(t), \quad i = 1, \dots, N, \quad (3)$$

where  $K_{pi}$  and  $K_{fi}$  are the controller's parameters.

The power request,  $P_{ci}(t)$ , can be expressed in the following static output feedback control structure [19]

$$P_{ci}(t) = K_{i1} f_i(t) + K_{i2} P_{tie,i}(t) + K_{i3} \vartheta_i(t), \quad (4)$$

where  $K_{i1}$ ,  $K_{i2}$ ,  $K_{i3}$  are the controller's parameters.

In this paper, we consider FDIA at the local control facility. Figure 2 shows how FDIA is implanted into LFC of ISGs. As mentioned previously, the area control error,  $ACE_i(t)$ , is necessary in the construction of power request command,  $P_{ci}(t)$ , in order to restore the stability of the closed loop system fluctuated by disturbances.  $ACE_i(t)$  is computed based on information of frequency,  $f_i(t)$ , and interchange power,  $P_{tie,i}(t)$ , hence, the hackers can degrade the LFC performance of the power grid [14, 15]. Their main strategy is to inject incorrect information,  $g_{i0}(t)$  during the process of computing  $ACE_i(t)$ . As a result, the counterfeit computed values of  $ACE_i^a(t)$  and its integral value are generated

$$\begin{aligned} ACE_i^a(t) &= P_{tie,i}(t) + b_i f_i(t) + g_{i0}(t) = ACE_i(t) + g_{i0}(t), \\ \vartheta_i^a(t) &= \int ACE_i^a(t) dt = \vartheta_i(t) + g_{i1}(t), \quad g_{i1}(t) = \int g_{i0}(t) dt. \end{aligned} \quad (5)$$

By which the computed control signal Equation (4) becomes

$$P_{ci}(t) = K_{i1} f_i(t) + K_{i2} P_{tie,i}(t) + K_{i3} \vartheta_i^a(t). \quad (6)$$

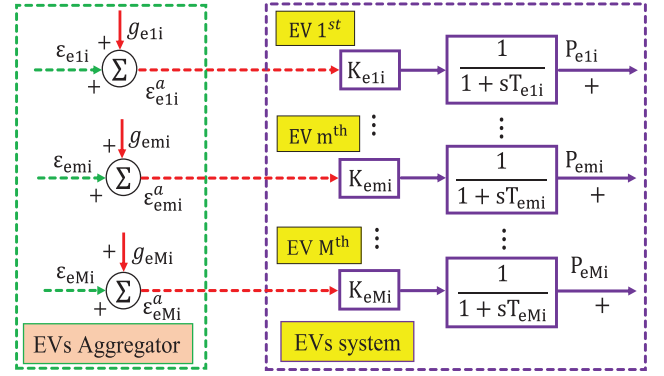


FIGURE 3 Block diagram of FDIA at the local aggregator of EVs

In this paper, we consider the operation of aggregated EVs. We assume that  $M$  of EVs are connected to power Area- $i^{\text{th}}$  to participate into LFC without state of charge control (SOC) [17]. An EV participates into LFC without SOC means that the output power of the EV,  $P_{emi}(t)$ , is determined by a constant EV gain,  $K_{emi}$ , as follows

$$\dot{P}_{emi}(t) = -\frac{1}{T_{emi}} \dot{P}_{emi}(t) + \frac{K_{emi}}{T_{emi}} \epsilon_{emi}(t) \quad (7)$$

where  $\epsilon_{emi}(t) = \epsilon_{ei}(t)/M$ ,  $\epsilon_{ei}(t) = -\rho_{ei} f_i(t - b_i)$ .  $K_{emi}$  and  $T_{emi}$  are gain and time constants of the  $m^{\text{th}}$  EV. Here we consider that all EVs have similar time constant,  $T_{emi} = T_{ei}$ .

The integration of an aggregated EVs requires a networked communication infrastructure with an aggregator (see Figure 3). This aggregator plays the role of a master to obtain the information of all individual EVs and allocate the individual power request command to them. Due to the existence of hacker actions, the request power signal for an individual EV,  $\epsilon_{emi}(t)$ , is changed by the injection of an incorrect information,  $g_{emi}(t)$ . Hence, a counterfeit command,  $\epsilon_{emi}^a(t) = \epsilon_{emi}(t) + g_{emi}(t)$ , is used for the EV instead of the true information,  $\epsilon_{emi}(t)$ . Therefore, the description of the EV taking FDIA into account is presented as follows

$$\begin{aligned} \epsilon_{emi}^a(t) &= -\frac{1}{M} \rho_{ei} f_i(t - b_i) + g_{emi}(t), \\ \dot{P}_{emi}^a(t) &= -\frac{1}{T_{emi}} \dot{P}_{emi}^a(t) + \frac{K_{emi}}{T_{emi}} \epsilon_{emi}^a(t) \\ &= -\frac{1}{T_{emi}} \dot{P}_{emi}^a(t) + \frac{K_{emi}}{T_{emi}} \left( \frac{1}{M} \epsilon_{ei}(t) + g_{emi}(t) \right). \end{aligned} \quad (8)$$

As a result, the output power of aggregated EVs,  $P_{ei}^a(t) = \sum_{m=1}^M P_{emi}^a(t)$  becomes

$$\begin{aligned} \dot{P}_{ei}^a(t) &= -\sum_{m=1}^M \frac{\dot{P}_{emi}^a(t)}{T_{ei}} + \sum_{m=1}^M \frac{K_{emi}}{MT_{ei}} \epsilon_{ei}(t) + \sum_{m=1}^M \frac{K_{emi}}{T_{ei}} g_{emi}(t) \\ &= -\frac{1}{T_{ei}} \dot{P}_{ei}^a(t) - \frac{K_{ei}}{T_{ei}} \rho_{ei} f_i(t - b_i) + \frac{K_{ei}}{T_{ei}} g_{i2}(t). \end{aligned} \quad (9)$$



where  $K_{ei} = \sum_{m=1}^M K_{emi}/M$  is the aggregated EVs gain.  $g_{i2}(t) = \sum_{m=1}^M (K_{emi}g_{emi}(t))/K_{ei}$  is considered as FDIAs on the aggregated EVs.

Accordingly, the equation of  $f_i(t)$  in Equation (1) becomes

$$\begin{aligned} \dot{f}_i(t) = & -\frac{D_i}{M_i}f_i(t) + \frac{1}{M_i}(P_{gi}(t) + P_{ei}^a(t) - P_{tie,i}(t)) \\ & -\frac{1}{M_i}(P_{li}(t) + P_{mi}(t)). \end{aligned} \quad (10)$$

In order to investigate the abnormal LFC operation of ISGs subject to multiple FDIAs, we develop the following state-space model of the studied system which encompasses the interactions of multiple communication delays, disturbances and FDIAs. First, we denote local state vector,  $x_i(t) \in \mathbb{R}^{n_i}$ , control input vector,  $u_i(t) \in \mathbb{R}$ , disturbance vector,  $d_i(t) \in \mathbb{R}$  and output vector,  $y_i(t) \in \mathbb{R}^{p_i}$  of the local power Area- $i$  as follows  $x_i(t) = [f_i(t) X_{gi}(t) P_{ri}(t) P_{gi}(t) P_{ei}^a(t) P_{tie,i}(t) \vartheta_i(t)]^T$ ,  $u_i(t) = P_{ei}(t)$ ,  $d_i(t) = P_{li}(t) + P_{mi}(t)$ ,  $y_i(t) = [f_i(t) P_{ei}^a(t) P_{tie,i}(t) \vartheta_i^a(t)]^T$ .

A state-space representation of the local power Area- $i^{\text{th}}$  is

$$\begin{aligned} \dot{x}_i(t) = & A_{ii}x_i(t) + A_{iib}x_i(t - b_i) + \sum_{j=1, j \neq i}^N A_{ij}x_j(t) \\ & + \Gamma_i d_i(t) + B_i u_i(t) + S_i g_i(t), \end{aligned} \quad (11)$$

$$y_i(t) = C_i x_i(t) + F_i g_i(t),$$

where  $g_i(t) = [g_{i1}(t) g_{i2}(t)]^T \in \mathbb{R}^2$ ,  $S_i = [S_{i1} S_{i2}]$ ,  $F_i = [F_{i1} F_{i2}]$ . System matrices  $A_{ii}, A_{iib} \in \mathbb{R}^{n_i \times n_i}$ ,  $A_{ij} \in \mathbb{R}^{n_i \times n_j}$ ,  $B_i, \Gamma_i, S_{i1}, S_{i2} \in \mathbb{R}^{n_i \times 1}$ ,  $C_i \in \mathbb{R}^{p_i \times n_i}$ ,  $F_{i1}, F_{i2} \in \mathbb{R}^{p_i \times 1}$  are given in the Appendix A.

Accordingly, a state-space model of  $N$ -area ISGs is obtained

$$\begin{aligned} \dot{x}(t) = & Ax(t) + \sum_{j=1, j \neq i}^N A_{ji}x_j(t - b_j) + \Gamma d(t) + Bu(t) + Sg(t), \\ y(t) = & Cx(t) + Fg(t), \end{aligned} \quad (12)$$

where  $x(t) = [x_1^T(t) \cdots x_N^T(t)]^T \in \mathbb{R}^n$ ,  $d(t) = [d_1(t) \cdots d_N(t)]^T \in \mathbb{R}^N$ ,  $u(t) = [u_1(t) \cdots u_N(t)]^T \in \mathbb{R}^N$ ,  $y(t) = [y_1^T(t) \cdots y_N^T(t)]^T \in \mathbb{R}^p$ ,  $g(t) = [g_1^T(t) \cdots g_N^T(t)]^T \in \mathbb{R}^{2N}$  are global state, disturbance, control input, output and FDIAs vectors. Matrices  $A, A_{ji} \in \mathbb{R}^{n \times n}$ ,  $B, \Gamma \in \mathbb{R}^{n \times N}$ ,  $S \in \mathbb{R}^{n \times 2N}$ ,  $C \in \mathbb{R}^{p \times n}$ ,  $F \in \mathbb{R}^{p \times 2N}$  are  $A = \begin{bmatrix} A_{11} & \cdots & A_{1N} \\ \vdots & \ddots & \vdots \\ A_{N1} & \cdots & A_{NN} \end{bmatrix}$ ,  $A_{ji} = \text{Diag}(0, \dots, A_{iib}, \dots, 0)$ ,  $B = \text{Diag}(B_1, \dots, B_N)$ ,  $\Gamma = \text{Diag}(\Gamma_1, \dots, \Gamma_N)$ ,  $C = \text{Diag}(C_1, \dots, C_N)$ ,  $S = \text{Diag}(S_1, \dots, S_N)$ ,  $F = \text{Diag}(F_1, \dots, F_N)$ .

**Remark 1.** In this paper, FDIAs in LFC take various forms: (i) counterfeit information of EVs power request,  $\varepsilon_{ei}(t)$  and (ii) injection of incorrect data into the process of computing the area error control signal,  $ACE_i(t)$  and its integral value,

$\vartheta_i(t) = \int ACE_i(t)dt$ . In the abnormal operation (ISGs subject to FDIAs), instead of reliable signals,  $P_{ei}(t)$  and  $\vartheta_i(t)$ , counterfeit information of  $P_{ei}^a(t)$  and  $\vartheta_i^a(t)$  are used for computing control input signals and other local monitoring functions. Therefore, system Equation (11) encompasses behaviours and interactions of a FDIA,  $g_{i1}(t)$ , in the output vector  $y_i(t)$ , and another FDIA,  $g_{i2}(t)$ , in dynamical equation of the system state vector,  $\dot{x}_i(t)$ ,  $x_i(t)$ . For the first time, a mathematical representation of ISGs considering multiple FDIAs, RES and time delays are derived in this paper. Hence, the state-space model Equation (11) is different to those previous works [14–16, 26]. In [14, 15], state space models of ISGs were not derived. In [16], the variations of REs and load demands were ignored. Furthermore, time delays were not considered in all of the previous works [14–16, 26].

When the FDIA,  $g_{i1}(t)$  and time delays are ignored, the state space model Equation (11) is converted to the model considered in [26]

$$\begin{aligned} \dot{x}_i(t) = & \bar{A}_{ii}x_i(t) + \sum_{j=1, j \neq i}^N A_{ij}x_j(t) + \Gamma_i d_i(t) + B_i u_i(t) \\ & + S_{i2}g_{i2}(t); \quad y_i(t) = C_i x_i(t), \end{aligned} \quad (13)$$

where  $\bar{A}_{ii} = A_{ii} + A_{iib}$ .

The main objective of this paper is to derive an effective detection method to detect and isolate FDIAs within ISGs. Each local detector is installed at the local power area to implement the tasks of detecting and isolating the local FDIAs only.

### 3 | DFO BASED DETECTION SCHEME FOR FDIAs

In this section, we develop a FDIAs detection method for ISGs. In this method, a local detector,  $\mathcal{D}_i$ , is placed at local Area- $i^{\text{th}}$  to detect the existence of local FDIAs,  $g_{i1}(t)$  and  $g_{i2}(t)$ , injected by hackers. At first, we propose a local residual generator,  $r_i(t)$ , which is used to construct the local detector at local power Area- $i^{\text{th}}$ ,  $i = 1, \dots, N$ ,

$$r_i(t) = T_i z_i(t) + E_i y_i(t). \quad (14)$$

In Equation (14),  $r_i(t) \in \mathbb{R}$  is a real function. Matrices  $T_i \in \mathbb{R}^{1 \times q_i}$ ,  $E_i \in \mathbb{R}^{1 \times p_i}$  are residual generator matrices that will be designed later.  $z_i(t) \in \mathbb{R}^{q_i}$  is computed based on the following DFO

$$\begin{aligned} \dot{z}_i(t) = & N_i z_i(t) + N_{ib} z_i(t - b_i) + J_i y_i(t) \\ & + J_{ib} y_i(t - b_i) + H_i u_i(t) + \sum_{j=1, j \neq i}^N J_{ij} \bar{y}_j(t), \end{aligned} \quad (15)$$

where  $N_i, N_{ib} \in \mathbb{R}^{q_i \times q_i}$ ,  $J_i, J_{ib} \in \mathbb{R}^{q_i \times p_i}$ ,  $J_{ij} \in \mathbb{R}^{q_i \times p_j}$ ,  $H_i \in \mathbb{R}^{q_i \times 1}$  are the observer gains and be determined such that  $z_i(t)$

asymptotically converges to a linear function of the local state vector,  $\hat{z}_i = L_i x_i(t)$  when there are no FDIAs within the power grid,  $g_i(t) = 0$ . In Equation (15),  $\bar{y}_j(t) = C_{ij}x_j(t) + \bar{F}_{ij}g_j(t)$  is a vector of the augmented outputs from neighbouring power areas, where  $C_{ij} \in \mathbb{R}^{p_{ij} \times n_j}$ ,  $\bar{F}_{ij} \in \mathbb{R}^{p_{ij} \times 2}$ .

For FDIAs detection purpose,  $T_i$ ,  $E_i$ ,  $L_i$  and DFO matrices should achieve the following detection requirements: (i) (safe case)  $\lim_{t \rightarrow \infty} r_i(t) = 0$  if  $g_i(t) = 0$ ; (ii) (unsafe case)  $\lim_{t \rightarrow \infty} r_i(t) \neq 0$  if  $g_i(t) \neq 0$ . We define  $\theta_i(t) = z_i(t) - L_i x_i(t)$  as the error between  $z_i(t)$  and  $\hat{z}_i(t)$ .

**Theorem 1.** *For any given control signal,  $u_i(t)$ , disturbance,  $d_i(t)$  and with no FDIAs,  $z_i(t)$  will asymptotically converge to  $\hat{z}_i = L_i x_i(t)$  if there exist matrices  $N_i$ ,  $N_{ib}$ ,  $J_i$ ,  $J_{ib}$ ,  $J_{ij}$ ,  $H_i$ ,  $L_i$  with appropriate dimensions satisfying*

$$\dot{\theta}_i(t) = N_i \theta_i(t) + N_{ib} \theta_i(t - b_i) \text{ is asymptotically stable,} \quad (16)$$

$$[\Omega_{i1} \ \Omega_{i2} \ \Omega_{i3} \ \Omega_{i4} \ \Omega_{i5} \ \Omega_{i6}] = 0, \quad (17)$$

where

$$\Omega_{i1} = -L_i \Gamma_i, \ \Omega_{i2} = N_i L_i + J_i C_i - L_i A_{ii}, \ \Omega_{i6} = [\Omega_{i6}^j], \ j \neq i,$$

$$\Omega_{i3} = N_{ib} L_i + J_{ib} C_i - L_i A_{ibb}, \ \Omega_{i4} = H_i - L_i B_i,$$

$$\Omega_{i5} = [\Omega_{i5}^j], \ j \neq i, \ \Omega_{i5}^j = J_{ij} C_{ij} - L_i A_{ij}, \ \Omega_{i6}^j = J_{ij} \bar{F}_{ij}.$$

*Proof of Theorem 1.* Let we define  $Y_i$ ,  $Y_{i1}$ ,  $Y_{i2}$  and  $\Omega_i$  which will be used later as  $Y_i = T_i L_i + E_i C_i$ ,  $Y_{i1} = J_i F_i - L_i S_i$ ,  $Y_{i2} = J_{ib} F_i$ ,  $Y_{i3} = E_i F_i$ ,  $\Omega_i = (J_i F_i - L_i S_i)g_i(t) + J_{ib} F_{ig_i}(t - b_i) = Y_{i1}g_i(t) + Y_{i2}g_i(t - b_i)$ .

Taking the derivative of  $\theta_i(t)$ , we obtain

$$\begin{aligned} \dot{\theta}_i(t) &= N_i \theta_i(t) + N_{ib} \theta_i(t - b_i) - L_i \Gamma_i d_i(t) \\ &\quad + (N_i L_i + J_i C_i - L_i A_{ii})x_i(t) + (H_i - L_i B_i)u_i(t) \\ &\quad + (N_{ib} L_i + J_{ib} C_i - L_i A_{ibb})x_i(t - b_i) \\ &\quad + (J_i F_i - L_i S_i)g_i(t) + J_{ib} F_{ig_i}(t - b_i) \\ &\quad + \sum_{j=1, j \neq i}^N (J_{ij} C_{ij} - L_i A_{ij})x_j(t) + \sum_{j=1, j \neq i}^N J_{ij} \bar{F}_{ij} g_j(t). \end{aligned} \quad (18)$$

$$\begin{aligned} \dot{\theta}_i(t) &= N_i \theta_i(t) + N_{ib} \theta_i(t - b_i) + \Omega_{i1} d_i(t) + \Omega_{i2} x_i(t) \\ &\quad + \Omega_{i3} x_i(t - b_i) + \Omega_{i4} u_i(t) + \Omega_i \\ &\quad + \sum_{j=1, j \neq i}^N \Omega_{i5}^j x_j(t) + \sum_{j=1, j \neq i}^N \Omega_{i6}^j g_j(t). \end{aligned} \quad (19)$$

For  $N_i$ ,  $N_{ib}$ ,  $J_i$ ,  $J_{ib}$ ,  $J_{ij}$  satisfying the conditions Equations (16) and (17) and with no FDIAs,  $g_i(t) = 0$ ,  $\Omega_i = 0$ , we have

$$\dot{\theta}_i(t) = N_i \theta_i(t) + N_{ib} \theta_i(t - b_i). \quad (20)$$

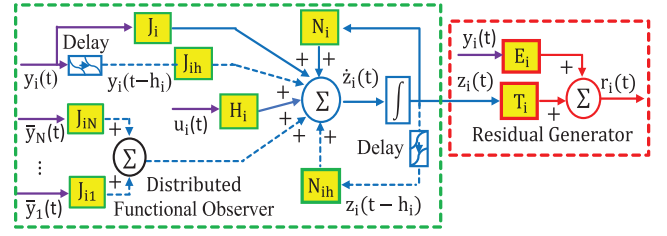


FIGURE 4 Schematic implementation of the proposed detector

As can be seen that Equation (20) is a time-delay system and  $\theta_i(t)$  will asymptotically converge to zero, ( $\theta_i(t) \rightarrow 0$ ), if the stability of Equation (20) is guaranteed (i.e. the condition Equations (16) and (17) are satisfied). This completes the proof of Theorem 1.  $\square$

It is noted that  $\theta_i(t) = z_i(t) - L_i x_i(t)$ . From Equation (14), the local residual generator,  $r_i(t)$ , can be rewritten in the following form

$$\begin{aligned} r_i(t) &= T_i(\theta_i(t) + L_i x_i(t)) + E_i(C_i x_i(t) + F_i g_i(t)) \\ &= T_i \theta_i(t) + (T_i L_i + E_i C_i)x_i(t) + E_i F_i g_i(t) \\ &= T_i \theta_i(t) + Y_i x_i(t) + Y_{i3} g_i(t), \end{aligned} \quad (21)$$

When  $Y_i = 0$ , Equation (21) becomes

$$r_i(t) = T_i \theta_i(t) + Y_{i3} g_i(t). \quad (22)$$

In the following part, according to Theorem 1, Equations (19) and (22) we propose a method using  $r_i(t)$  to detect local FDIAs.

- i When no FDIA exist within the systems ( $\Omega_i = 0$  and  $Y_{i3} g_i(t) = 0$ ) and Theorem 1 is satisfied, residual generator,  $r_i(t) \rightarrow 0$  as  $t \rightarrow \infty$ .
- ii In contrast, when FDIAs exist in the system,  $\Omega_i \neq 0$  or  $Y_{i3} g_i(t) \neq 0$ , and Theorem 1 is satisfied,  $r_i(t)$  will not asymptotically converge to 0, ( $r_i(t) \not\rightarrow 0$ ).

Therefore, residual generator,  $r_i(t)$ , can be used as an indicator for FDIAs detection purpose. The schematic implementation of DFO based FDIAs detection method is shown on Figure 4. In this scheme, a detector (a residual generator based observer) is located at the local power Area- $i^{\text{th}}$  to detect its FDIAs. The residual value is computed according to matrices  $T_i$ ,  $E_i$  together with a DFO.

In the following, we develop corollary 1 such that  $r_i(t)$  reacts to FDIAs ( $r_i(t) \not\rightarrow 0$ ).

**Corollary 1.** *Local residual generator,  $r(t) \not\rightarrow 0$  as  $t \rightarrow \infty$  for any local FDIAs,  $g_{i1}(t)$ ,  $g_{i2}(t)$ , if the following conditions are satisfied*

$$\begin{aligned} Y_i &= 0, \text{ Diag}(Y_{i1}^1, Y_{i2}^1, Y_{i3}^1) \neq 0, \\ \text{Diag}(Y_{i1}^2, Y_{i2}^2, Y_{i3}^2) &\neq 0, \end{aligned} \quad (23)$$

where  $\mathbf{Y}_{i1} = [\mathbf{Y}_{i1}^1 \ \mathbf{Y}_{i1}^2]$ ,  $\mathbf{Y}_{i1}^1 = J_i F_{i1} - L_i S_{i1}$ ,  $\mathbf{Y}_{i1}^2 = J_i F_{i2} - L_i S_{i2}$ ,  $\mathbf{Y}_{i2} = [\mathbf{Y}_{i2}^1 \ \mathbf{Y}_{i2}^2]$ ,  $\mathbf{Y}_{i2}^1 = J_{ib} F_{i1}$ ,  $\mathbf{Y}_{i2}^2 = J_{ib} F_{i2}$ ,  $\mathbf{Y}_{i3} = [\mathbf{Y}_{i3}^1 \ \mathbf{Y}_{i3}^2]$ ,  $\mathbf{Y}_{i3}^1 = E_i F_{i1}$ ,  $\mathbf{Y}_{i3}^2 = E_i F_{i2}$ .

*Proof of Corollary 1.* Let us consider  $\mathbf{Y}_i$ ,  $\mathbf{Y}_{i1}^1$ ,  $\mathbf{Y}_{i2}^1$ ,  $\mathbf{Y}_{i3}^1$ ,  $\mathbf{Y}_{i1}^2$ ,  $\mathbf{Y}_{i2}^2$ ,  $\mathbf{Y}_{i3}^2$  satisfying Corollary 1. We assume that only  $g_{i1}(t)$  exists at the local power Area- $i^{th}$  such  $g_{i1}(t) \neq 0$ ,  $g_{i2}(t) = 0$ . According to Corollary 1, we have one of the terms  $\mathbf{Y}_{i1}^1 g_{i1}(t)$ ,  $\mathbf{Y}_{i2}^1 g_{i1}(t)$  and  $\mathbf{Y}_{i3}^1 g_{i1}(t)$  is not zero. Therefore  $\Omega_i \neq 0$  or  $\mathbf{Y}_{i3} g_{i1}(t) \neq 0$  leading to  $r_i(t) \rightarrow 0$  as  $t \rightarrow \infty$ . The proof can be applied to  $g_{i2}(t)$ . This completes the proof of Corollary 1.  $\square$

*Remark 2.* We consider model Equation (11) where  $g_{i1}(t) = 0$ ,  $b_i = 0$ . By using a similar structure of DFO and residual generator form in Equations (14)-(15), a detector for Equation (11) can be developed.

$$\dot{\hat{z}}_i(t) = N_i \hat{z}_i(t) + J_i y_i(t) + H_i u_i(t) + \sum_{j=1, j \neq i}^N J_{ij} \hat{y}_j(t). \quad (24)$$

The derivative of  $\theta_i(t)$  is  $\dot{\theta}_i(t) = N_i \theta_i(t) - L_i S_{i2} g_{i2}(t)$ . The local residual generator is  $r_i(t) = T_i \theta_i(t) + \mathbf{Y}_i x_i(t)$ . Therefore,  $r_i(t)$  reacts to  $g_{i2}(t)$ , if the Theorem 1 holds,  $\mathbf{Y}_i = 0$  and the following condition is satisfied  $L_i S_{i2} \neq 0$ . This completes Remark 2.

*Remark 3.* Along with FDIAs detection, isolation of FDIAs is also very important in monitoring system. The information of FDIAs isolation can be used to improve the monitoring function of ISGs to determine further action to handle the FDIAs. Here, together with Theorem 1, we consider conditions such that local residual generator,  $r_i(t)$ , be insensitive to a local FDIA. ‘‘Insensitive’’ refers to a situation that if an FDIA happens, the detector does not react to that attack.

**Corollary 2.** When Theorem 1 holds and  $\mathbf{Y}_i = 0$ ,  $r_i(t)$  is insensitive to a local FDIA,  $g_{ik}(t)$ , if there exist matrices  $\mathbf{Y}_{i1}^k$ ,  $\mathbf{Y}_{i2}^k$ ,  $\mathbf{Y}_{i3}^k$  such that the following conditions are satisfied

$$\text{Diag}(\mathbf{Y}_{i1}^k, \mathbf{Y}_{i2}^k, \mathbf{Y}_{i3}^k) = 0. \quad (25)$$

where  $\mathbf{Y}_{i1}^k$ ,  $\mathbf{Y}_{i2}^k$  and  $\mathbf{Y}_{i3}^k$  are given in Corollary 1.

*Proof of Corollary 2.* The proof can be obtained by using similar lines as in the proof of Corollary 1. Hence, we omit it here.

By using Corollary 2, we can build extra detectors- $\mathcal{D}_{ik}$ ,  $k = 1, 2$ , where  $\mathcal{D}_{ik}$  includes a residual generator,  $r_{ik}(t)$ ,  $k = 1, 2$ , which is insensitive to the FDIA of  $g_{ik}(t)$  while it is sensitive to the remaining local FDIA. By using the extra detectors together with the main detector  $\mathcal{D}_i$  (residual  $r_i(t)$ ), FDIAs can be isolated.

This completes Remark 2.  $\square$

*Remark 4.* In this Remark, we develop a CFO based FDIAs detection method for ISGs. In this design, a centralised global detector,  $\mathcal{D}$ , will detect the happening of all FDIAs. A global

residual generator,  $r(t) \in \mathbb{R}$ , which is used to form the global detector.

$$r(t) = T\hat{z}(t) + E y(t). \quad (26)$$

In Equation (26),  $T \in \mathbb{R}^{1 \times q}$ ,  $E \in \mathbb{R}^{1 \times p}$  are residual generator's matrix gains.  $\hat{z}(t) \in \mathbb{R}^q$  is computed based on structure of CFO

$$\begin{aligned} \dot{\hat{z}}(t) = & \bar{N}\hat{z}(t) + \sum_{i=1}^N N_{bi} \hat{z}(t - b_i) + \sum_{i=1}^N J_{bi} y(t - b_i) \\ & + J y(t) + H u(t), \end{aligned} \quad (27)$$

where  $\bar{N}$ ,  $N_{bi} \in \mathbb{R}^{q \times q}$ ,  $J, J_{bi} \in \mathbb{R}^{q \times p}$ ,  $H \in \mathbb{R}^{q \times m}$  are the CFO gains and be determined such that  $\hat{z}(t)$  asymptotically converges to a linear functional of the local state vector,  $\hat{z} = Lx(t)$  when there are no FDIAs within the ISG,  $g(t) = 0$ .

For the detection purpose,  $T$ ,  $E$ ,  $L$  and CFO matrices should achieve the following detection requirements: (i) (safe case)  $\lim_{t \rightarrow \infty} r(t) = 0$  if  $g(t) = 0$ ; (ii) (unsafe case)  $\lim_{t \rightarrow \infty} r(t) \neq 0$  if  $g(t) \neq 0$ .  $\theta(t) = \hat{z}(t) - Lx(t)$  as the error between  $\hat{z}(t)$  and  $\hat{z}(t)$ .

**Corollary 3.** For any given control signal,  $u(t)$ , disturbance,  $d(t)$  and with no FDIAs,  $\hat{z}(t)$  asymptotically converges to  $\hat{z}(t) = Lx(t)$  if there exist matrices  $\bar{N}$ ,  $N_{bi}$ ,  $J$ ,  $J_{bi}$ ,  $L$  with appropriate dimensions satisfying

$$\begin{aligned} \dot{\theta}(t) = & \bar{N}\theta(t) + \sum_{i=1}^N N_{bi} \theta(t - b_i) \text{ is asymptotically stable,} \\ [\Omega_1 \ \Omega_2 \ \Omega_3 \ \Omega_4] = & 0, \end{aligned} \quad (28)$$

where  $\Omega_1 = -L\bar{N}$ ,  $\Omega_2 = \bar{N}L + JC - LA$ ,  $\Omega_3 = [\Omega_{3i}]$ ,  $\Omega_{3i} = N_{bi}L + J_{bi}C - LA_{bi}$ ,  $\Omega_4 = H - LB$ .

*Proof of Corollary 3.* We define  $\mathbf{Y} = TL + EC$ ,  $\mathbf{Y}_1 = JF - LS$ ,  $\mathbf{Y}_{2i} = J_{bi}F$ ,  $\mathbf{Y}_3 = EF$ ,  $\Omega = \mathbf{Y}_1 g(t) + \sum_{i=1}^N \mathbf{Y}_{2i} g(t - b_i)$ .

We have  $\dot{\theta}(t) = \bar{N}\theta(t) + \sum_{i=1}^N N_{bi} \theta(t - b_i) + \sum_{i=1}^N \Omega_{3i} x(t - b_i) + \Omega_1 d(t) + \Omega_2 x(t) + \Omega_4 u(t) + \Omega$ .

For  $\bar{N}$ ,  $N_{bi}$ ,  $J$ ,  $J_{bi}$  satisfying Equation (28) and with no FDIAs,  $g(t) = 0$ ,  $\Omega = 0$ , we obtain  $\dot{\theta}(t) = \bar{N}\theta(t) + \sum_{i=1}^N N_{bi} \theta(t - b_i)$ . This is a linear system with multiple time delays and  $\theta(t)$  will asymptotically converge to zero, ( $\theta(t) \rightarrow 0$ ), if the stability is guaranteed. This completes the proof of Corollary 3.  $\square$

The residual generator is  $r(t) = T\theta(t) + \mathbf{Y}x(t) + \mathbf{Y}_3 g(t)$ . When  $\mathbf{Y} = 0$ ,  $r(t)$  becomes  $r(t) = T\theta(t) + \mathbf{Y}_3 g(t)$ . Now, according to Corollary 3, we propose a method using  $r(t)$  to detect FDIAs. When no FDIAs exist within the systems ( $\Omega = 0$  and  $\mathbf{Y}_3 g(t) = 0$ ) and Corollary 3 is satisfied, residual generator,  $r(t) \rightarrow 0$  as  $t \rightarrow \infty$ . In contrast, when FDIAs exist in the system,  $\Omega \neq 0$  or  $\mathbf{Y}_3 g(t) \neq 0$ , and Corollary 3 is satisfied,  $r(t)$  will not asymptotically converge to 0, ( $r(t) \rightarrow 0$ ).

**Corollary 4.** *Residual generator,  $r(t) \nrightarrow 0$  as  $t \rightarrow \infty$  for any FDLAs, if the following conditions are satisfied*

$$Y = 0, \text{Diag}(Y_1^k, Y_2^k, Y_3^k) \neq 0, k = 1, \dots, 2N, \quad (29)$$

where  $Y_1 = [Y_1^1 \dots Y_1^{2N}]$ ,  $Y_1^k = JF^k - LS^k$ ,  $Y_2 = [Y_{2i}]$ ,  $Y_{2i} = [Y_{2i}^1 \dots Y_{2i}^{2N}]$ ,  $Y_{2i}^k = J_{bi}F^k$ ,  $Y_3 = [Y_3^1 \dots Y_3^{2N}]$ ,  $Y_3^k = EF^k \cdot S^k$ ,  $F^k$  is  $k^{\text{th}}$  columns of  $S$  and  $F$ .

*Proof of Corollary 4.* The proof for this Corollary can be obtained by using a similar technique in Corollary 1, hence we omit here. This completes Corollary 4 and Remark 4.  $\square$

## 4 | DFO BASED DETECTOR SYNTHESIS

We now in the step to develop a procedure to synthesis the unknown parameters of detector- $\mathcal{D}_i$ ,  $T_i$ ,  $L_i$ ,  $E_i$ ,  $N_i$ ,  $N_{ib}$ ,  $J_i$ ,  $J_{ib}$ ,  $J_{ij}$  and  $H_i$  in Equations (14)-(15). Let we introduce following Lemmas 1 and 2 which are necessary for the synthesis procedure of  $\mathcal{D}_i$ .

**Lemma 1** ([34]). *We consider a linear equation  $X\Omega_1 = \Omega_2$ ,  $X \in \mathbb{R}^{n \times p}$ ,  $\Omega_1 \in \mathbb{R}^{p \times m}$ ,  $\Omega_2 \in \mathbb{R}^{n \times m}$ . There exists a solution  $X$  if and only if*

$$\text{rank}\left(\begin{bmatrix} \Omega_2 \\ \Omega_1 \end{bmatrix}\right) = \text{rank}(\Omega_1), \quad (30)$$

and  $X$  can be obtained as  $X = \Omega_2\Omega_1^+ + Z(I_p - \Omega_1\Omega_1^+)$  where  $\Omega_1^+$  is the Moore-Penrose inverse of  $\Omega_1$ ,  $Z \in \mathbb{R}^{n \times p}$  is an arbitrary matrix.

**Lemma 2** ([33]). *We consider the homogenous linear equation*

$$Y\Omega = 0, \quad (31)$$

where  $Y \in \mathbb{R}^{n \times m}$  is an unknown matrix,  $\Omega \in \mathbb{R}^{m \times p}$  is a known matrix.

The Equation (31) has nontrivial solutions if  $v < m$ , where  $\text{rank}(\Omega) = v$  and  $Y$  can be taken from any rows of the following matrix  $\bar{Y} = \mathcal{N}(\Omega)$ , where  $\mathcal{N}(\Omega)$  is the matrix of row basis vectors for the row nullspace of  $\Omega$  such  $\mathcal{N}(\Omega)\Omega = 0$ .

In this position of paper, we derive a stability condition for linear time delay system Equation (20) which presents the DFO error,  $\hat{\theta}_i(t) = N_i\theta_i(t) + N_{ib}\theta_i(t - b_i)$ . The stability condition is established by using Lyapunov stability for time-delay system, Refine Jensen matrix inequality [35] and free-weighting matrix technique.

**Theorem 2.** *For given scalars  $b_i$ ,  $\delta_i$ , and matrices  $N_i, N_{ib} \in \mathbb{R}^{q_i \times q_i}$ , system Equation (20) is asymptotically stable if there exist positive definite matrices  $P_i, Q_i, R_i \in \mathbb{R}^{q_i \times q_i}$ , and a matrix  $X_i \in \mathbb{R}^{q_i \times q_i}$  satisfying the following matrix inequality*

$$\Lambda_i = \Lambda_{i1} + \Lambda_{i2} + \Lambda_{i3} + \Lambda_{i4} < 0, \quad (32)$$

where  $\Lambda_{i1} = e_{i1}^T P_i e_{i2} + e_{i2}^T P_i e_{i1}$ ,  $\Lambda_{i2} = e_{i1}^T Q_i e_{i1} - e_{i3}^T Q_i e_{i3} + e_{i2}^T (b_i^2 R_i) e_{i2}$ ,  $\Lambda_{i3} = -F_i^T R_i F_i$ ,  $\Lambda_{i4} = \mathcal{M}_i \mathcal{N}_i + \mathcal{N}_i^T \mathcal{M}_i^T$ ,  $\mathcal{M}_i = (e_{i1}^T + \delta_i e_{i2}^T)$ ,  $\mathcal{N}_i = -X_i e_{i2} + X_i N_i e_{i1} + X_i N_{ib} e_{i3}$ ,  $e_{il} = [0_{q_i \times l_{q_i}} \ I \ 0_{q_i \times (4-l)_{q_i}}]$ ,  $0 \leq l \leq 4$ ,  $F_i = [F_{i1}^T \ F_{i2}^T \ F_{i3}^T]^T$ ,  $F_{i1} = e_{i1} - e_{i3}$ ,  $R_i = \text{Diag}(R_i, 3R_i, 5R_i)$ ,  $F_{i2} = e_{i1} + e_{i3} - 2e_{i4}$ ,  $F_{i3} = e_{i1} - e_{i3} + 6e_{i4} - 6e_{i5}$ .

*Proof of Theorem 2.* We denote some following notations

$$\chi_i(t) = [\theta_i^T(t) \ \dot{\theta}_i^T(t) \ \chi_{i1}^T(t) \ \chi_{i2}^T(t) \ \chi_{i3}^T(t)]^T, \quad \chi_{i1}(t) = \theta_i(t - b_i), \chi_{i2}(t) = \frac{1}{b_i} \int_{t-b_i}^t \theta_i(s) ds, \chi_{i3}(t) = 2/b_i^2 \int_{-b_i}^0 \int_{t+s}^t \theta_i(u) du ds.$$

We construct the Lyapunov-Krasovskii functional candidate:  $V_i(\theta_i(t), t) = \theta_i^T(t) P_i \theta_i(t) + \int_{t-b_i}^t \theta_i^T(s) Q_i \theta_i(s) ds + b_i \int_{-b_i}^0 \int_{t+s}^t \dot{\theta}_i^T(u) R_i \dot{\theta}_i(u) du ds$ .

By taking the derivative of  $V_i(\theta_i(t), t)$ , we obtain  $\dot{V}_i(\theta_i(t), t) = \chi_i^T(t) (\Lambda_{i1} + \Lambda_{i2}) \chi_i(t) - b_i \int_{t-b_i}^t \dot{\theta}_i^T(s) R_i \dot{\theta}_i(s) ds$ . Now we use the refined Jensen inequality [35] to derive the following estimation  $-b_i \int_{t-b_i}^t \dot{\theta}_i^T(s) R_i \dot{\theta}_i(s) ds \leq \chi_i^T(t) \Lambda_{i3} \chi_i(t)$ . We apply free-weighting matrix for system Equation (20) to obtain  $2\theta_i^T(t) + \delta_i \dot{\theta}_i^T(t) X_i \times [N_i \theta_i(t) + N_{ib} \theta_i(t - b_i) - \dot{\theta}_i(t)] = 0$ . Adding the left-hand side of above equation to  $\dot{V}_i(\theta_i(t), t)$ , we have

$$\dot{V}_i(\theta_i(t), t) \leq \chi_i^T(t) \Lambda_i \chi_i(t). \quad (33)$$

If condition in Equation (32) holds if  $\Lambda_i < 0$  then  $\dot{V}_i(\theta_i(t), t) < 0$ . Therefore, system Equation (20) is asymptotically stable. This completes proof of Theorem 2.  $\square$

Now we are in the main stage of this section. In this step, we solve the condition presented in Theorem 1 and corollary 1 for the exits of proposed detector,  $\mathcal{D}_i$ . By solving these conditions, the detector's parameters ( $N_i, N_{ib}, J_i, J_{ib}, J_{ij}, T_i, H_i$  and  $E_i$ ) can be obtained. To solve these conditions, above Lemma 1, Lemma 2 and Theorem 2 will be used. For the ease of presentation, we present the process of solving Equations (16), (17) and (32) in a procedure of four main steps which can be implemented by using various of computation tools.

### Detector synthesis procedure:

**Step 1:** Solve  $\Omega_{i1} = 0$ ,  $\Omega_{i4} = 0$ ,  $\Omega_{i5} = 0$  in Theorem 1 to obtain  $L_i, J_{ij}, j = 1, \dots, N, j \neq i$ , then  $H_i$ . Let we denote  $\Xi_i = \begin{bmatrix} \Xi_{ia} & 0 \\ -\Xi_{ib} & \Gamma_i \end{bmatrix}$ , where  $\Xi_{ia} = \text{Diag}(C_{i1}, \dots, C_{i(i-1)}, C_{i(i+1)}, \dots, C_{iN})$ ,  $C_{ij} \in \mathbb{R}^{b_{ij} \times n_i}$ ,  $\Xi_{ib} = [A_{i1} \dots A_{i(i-1)} \ A_{i(i+1)} \dots A_{iN}]$ ,  $\Xi_{ic} = [J_{i1} \dots J_{i(i-1)} \ J_{i(i+1)} \dots J_{iN}]$ ,  $\Psi_i = [\Xi_{ic} \ L_i]$ ,  $\tilde{P}_i = \sum_{j=1, j \neq i}^N \tilde{p}_{ij}$ . From  $\Omega_{i1} = 0$  and  $\Omega_{i5} = 0, j \neq i$  in Equations (16)-(17), we obtain the following equality

$$\Psi_i \Xi_i = 0, \quad (34)$$

Equation (34) has solution if  $\Psi_i$ , if  $\Xi_i$  satisfies Lemma 2. To do that, we use Matlab software with “rank” command to check  $\text{rank}(\Xi_i) < (\tilde{p}_i + n_i)$ , then  $\Psi_i$  can be obtained by taking some rows of  $\tilde{\Psi}_i = \mathcal{N}(\Xi_i)$ . Here the DFO parameter,  $J_{ij}$  and matrix



$L_i$  can be obtained from  $\Psi_i$ . Finally,  $H_i$  is obtained from  $\Omega_{i4} = 0$  in Equations (16) and (17),  $H_i = L_i B_i$ .

**Step 2:** To solve conditions of  $\Omega_{i2}$  and  $\Omega_{i3}$  in Theorem 1 for the existence of  $N_i, N_{ib}, J_i, J_{ib}$ . We denote  $\Phi_{i2} = [L_i A_{ii} \ L_i A_{iib}]$  and  $\Phi_{i1} = \text{diag}(\tilde{\Xi}_i, \tilde{\Xi}_i)$ , where  $\tilde{\Xi}_i = [L_i^T \ C_i^T]^T$ . From  $\Omega_{i2} = 0$  and  $\Omega_{i3} = 0$  in Equations (16)-(17), we obtain the following results

$$[N_i \ J_i \ N_{ib} \ J_{ib}] \Phi_{i1} = \Phi_{i2}. \quad (35)$$

According to Lemma 1, Equation (35) has solution if it satisfies the following condition of matrix rank.  $\text{rank} \begin{bmatrix} \Phi_{i2}^T & \Phi_{i1}^T \end{bmatrix}^T = \text{rank}(\Phi_{i1})$ . If this condition of rank  $\Phi_{i2}, \Phi_{i1}$  are satisfied, detector's matrices  $N_i, N_{ib}, J_i, J_{ib}$  can be rewritten in the following structure

$$= \Phi_{i2} \Phi_{i1}^+ + Z_i (I_{2(p_i+q_i)} - \Phi_{i1} \Phi_{i1}^+), \quad (36)$$

where  $N_i = N_{i1} + Z_i N_{i2}$ ,  $N_{ib} = N_{ib1} + Z_i N_{ib2}$ ,  $J_i = J_{i01} + Z_i J_{i02}$ ,  $J_{ib} = J_{ib1} + Z_i J_{ib2}$ ,  $\Phi_{i1}^+$  is the Moore–Penrose pseudoinverse of  $\Phi_{i1}$ .  $Z_i$  will be obtained later and  $N_{i1}, N_{i2}, N_{ib1}, N_{ib2}, J_{i1}, J_{i2}, J_{ib1}, J_{ib2}$  are

$$N_{i1} = \Phi_{i2} \Phi_{i1}^+ \lambda_{i1}, \quad N_{i2} = (I_{2p_i+2q_i} - \Phi_{i1} \Phi_{i1}^+) \lambda_{i1},$$

$$J_{i01} = \Phi_{i2} \Phi_{i1}^+ \lambda_{i2}, \quad J_{i02} = (I_{2p_i+2q_i} - \Phi_{i1} \Phi_{i1}^+) \lambda_{i2},$$

$$N_{ib1} = \Phi_{i2} \Phi_{i1}^+ \lambda_{i3}, \quad N_{ib2} = (I_{2p_i+2q_i} - \Phi_{i1} \Phi_{i1}^+) \lambda_{i3},$$

$$J_{ib1} = \Phi_{i2} \Phi_{i1}^+ \lambda_{i4}, \quad J_{ib2} = (I_{2p_i+2q_i} - \Phi_{i1} \Phi_{i1}^+) \lambda_{i4},$$

$$\lambda_{i1} = [I_{q_i} \ 0_{q_i \times (q_i+2p_i)}]^T, \lambda_{i2} = [0_{p_i \times q_i} \ I_{p_i} \ 0_{p_i \times (q_i+p_i)}]^T,$$

$$\lambda_{i3} = [0_{q_i \times (q_i+p_i)} \ I_{q_i} \ 0_{q_i \times p_i}]^T, \lambda_{i4} = [0_{p_i \times (2q_i+p_i)} \ I_{p_i}]^T.$$

As can be seen that, after some calculations, we have presented  $N_i, N_{ib}$  by some matrices where  $N_{i1}, N_{i2}, N_{ib1}, N_{ib2}$  are known and  $Z_i$  need be calculated. Then, the equation for DFO error,  $\theta_i(t)$  in Equation (20) becomes the following construction

$$\dot{\theta}_i(t) = (N_{i1} + Z_i N_{i2}) \theta_i(t) + (N_{ib1} + Z_i N_{ib2}) \theta_i(t - h_i). \quad (37)$$

**Step 3:** we derive  $Z_i$  such Equation (37) is asymptotically stable, then we obtain  $N_i, N_{ib}, J_i, J_{ib}$  from Equation (37). To do that, we develop the following Corollary 5 for synthesising  $Z_i$ . The corollary 5 is derived according to Theorem 2. Roughly speaking, corollary 5 is a presentation of Theorem 2 in a tractable LMI form, therefore, which can be solved automatically by LMI solver in MATLAB.

**Corollary 5.** For given positive scalars  $h_i$  and  $\delta_i$ , system Equation (37) is asymptotically stable if there exist positive definite matrices  $P_i, Q_i, R_i \in \mathbb{R}^{q_i \times q_i}$  and matrices  $X_i, Y_i$  with appropriate dimension satisfying the following LMI

$$\bar{\Lambda}_i = \Lambda_{i1} + \Lambda_{i2} + \Lambda_{i3} + \bar{\Lambda}_{i4} < 0, \quad (38)$$

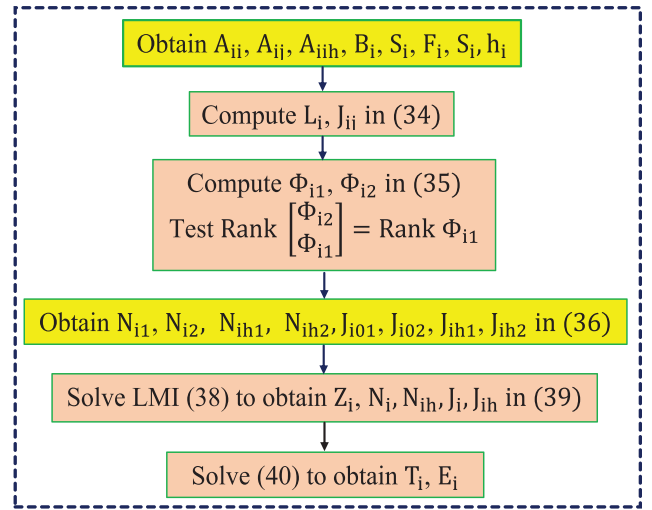


FIGURE 5 Detector synthesis procedure

where  $\bar{\Lambda}_{i4} = \mathcal{M}_i \bar{\mathcal{N}}_i + \bar{\mathcal{N}}_i^T \mathcal{M}_i^T$ ,  $\bar{\mathcal{N}}_i = -X_i e_{i2} + X_i N_{i1} e_{i1} + Y_i N_{i2} e_{i1} + X_i N_{ib1} e_{i3} + Y_i N_{ib2} e_{i3}$ ,  $e_{i1}, \Lambda_{i1}, \Lambda_{i2}, \Lambda_{i3}, \mathcal{M}_i$  are from the Theorem 2.

*Proof of Corollary 5.* Let we define  $Y_i = X_i Z_i$ , the apply  $N_i = N_{i1} + Z_i N_{i2}$ ,  $N_{ib} = N_{ib1} + Z_i N_{ib2}$ , we can obtain Equation (32). It shows that LMI Equation (32) hold if LMI Equation (38) holds. This completes proof of Corollary 5.  $\square$

By using robust control toolbox in Malab to solve the LMI Equation (38),  $Z_i$  and detector gains  $N_i, N_{ib}, J_i, J_{ib}$  can be obtained as

$$\begin{aligned} Z_i &= X_i^{-1} Y_i, N_i = N_{i1} + Z_i N_{i2}, N_{ib} = N_{ib1} + Z_i N_{ib2}, \\ J_i &= J_{i01} + Z_i J_{i02}, J_{ib} = J_{ib1} + Z_i J_{ib2}. \end{aligned} \quad (39)$$

This completes Step 3 of the procedure.

**Step 4:** We solve condition of  $Y_i = 0$  in Corollary 1 to obtain residual generator gains  $T_i$  and  $E_i$ . Let we denote  $\Sigma_i = [T_i \ E_i]$ . From  $\tilde{\Xi}_i$  derived in Step 2 of this procedure and the condition of  $Y_i = 0$  in Equation (23), we obtain the following result

$$\Sigma_i \tilde{\Xi}_i = 0. \quad (40)$$

From Lemma 2, we use MATLAB software test  $\text{rank}(\tilde{\Xi}_i) < q_i + p_i$ . Thus  $T_i, E_i$  are taken from rows of  $\tilde{\Sigma}_i = \mathcal{N}(\tilde{\Xi}_i)$ . Finally, we test the conditions  $\text{Diag}(Y_{i1}^1, Y_{i2}^1, Y_{i3}^1) \neq 0$ ,  $\text{Diag}(Y_{i1}^2, Y_{i2}^2, Y_{i3}^2) \neq 0$  in Equation (23). If all two conditions are not satisfied, the residual generator is insensitive to both FDIA's whereas if one of them is satisfied, the residual generator is sensitive to one FDIA and insensitive to other, go back to choose another value of  $L_i$  in Step 1. Otherwise, this completes the detector synthesis procedure. The procedure is demonstrated in Figure 5.

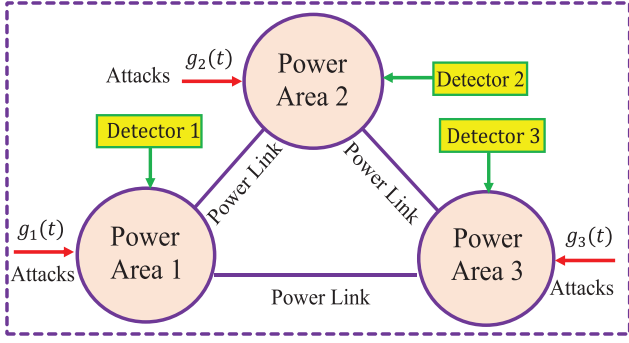


FIGURE 6 Architecture of three-area ISGs with DFO detectors

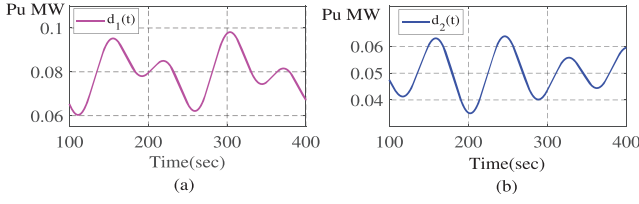


FIGURE 7 Intermittent of RES powers and demand: (a)  $d_1(t)$ , (b)  $d_2(t)$

## 5 | RESULTS AND DISCUSSION

### 5.1 | Stability of LFC for ISGs

#### 5.1.1 | LFC of time delay ISGs

In this section, a three-area ISG with reheated thermal power plants, delayed EVs and RES are used for demonstrating our detection method. The intermittent of RES and demand changes are formulated as following time-varying functions  $d_i(t) = d_{0i} + d_{1i} \sin(\phi_{1i}t) + d_{2i} \cos(\phi_{2i}t)$  puMW, where  $d_{0i}$ ,  $d_{1i}$ ,  $d_{2i}$ ,  $\phi_{1i}$ ,  $\phi_{2i}$ ,  $i = 1, 2, 3$  are the magnitudes of load demand, RES and the frequencies of the functions as follows  $d_{01} = 0.08$ ,  $d_{11} = 0.01$ ,  $d_{21} = 0.01$ ,  $\phi_{11} = \sqrt{0.002}$ ,  $\phi_{21} = \sqrt{0.007}$ ,  $d_{02} = 0.05$ ,  $d_{12} = 0.005$ ,  $d_{22} = 0.01$ ,  $\phi_{12} = \sqrt{0.003}$ ,  $\phi_{22} = \sqrt{0.006}$ ,  $d_{03} = 0.13$ ,  $d_{13} = 0.01$ ,  $d_{23} = 0.005$ ,  $\phi_{13} = \sqrt{0.005}$ ,  $\phi_{23} = \sqrt{0.004}$ . The demonstration of  $d_1(t)$  and  $d_2(t)$  are provided in Figure 6. Other parameters of studied systems can be gathered from Appendix. The system control input signals,  $u_i(t)$ ,  $i = 1, 2, 3$  can be obtained by following computation  $u_i(t) = K_{i1}f_i(t) + K_{i2}P_{tie,i}(t) + K_{i3}\vartheta_i(t)$ , where  $K_{i2} = 0.1$ ,  $K_{i1} = b_i K_{i2} = 0.0425$ ,  $K_{i3} = -0.1$  are LFC controller gains. Time delays,  $b_i = b = 0.1$ s.

We undertook Scenario I to show that above controller is adequate to achieve the main objectives of LFC in normal operation of the ISG (without FDIAs,  $g(t) = 0$ ). Figures 8 and 9 illustrate the responses of frequency deviations,  $f_i(t)$ , and interchange power deviations,  $P_{tie,i}(t)$ ,  $i = 1, 2, 3$  of closed-loop systems for the duration of 180 seconds (from the second of 140 to 320) of simulation. These simulation results indicate that  $f_i(t)$  and  $P_{tie,i}(t)$  are brought back in very small bounds of desirable value,  $f_1(t) \in [-0.0062, 0.0039]$  Hz,  $f_2(t) \in [-0.0077, 0.0055]$

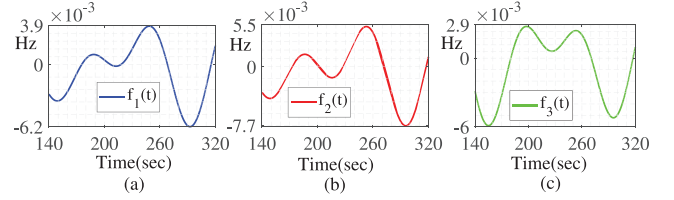


FIGURE 8 The responses of  $f_i(t)$  (Scenario I): (a)  $f_1(t)$ , (b)  $f_2(t)$ , (c)  $f_3(t)$

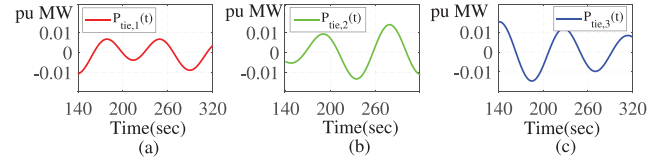


FIGURE 9 The responses of  $P_{tie,i}(t)$  (Scenario I): (a)  $P_{tie,1}(t)$ , (b)  $P_{tie,2}(t)$ , (c)  $P_{tie,3}(t)$

Hz,  $f_3(t) \in [-0.006, 0.0029]$  Hz,  $P_{tie,i}(t)$ ,  $i = 1, 2, 3$  belongs to a range of  $[-0.01, 0.01]$  puMW which is corresponding to 10% of fluctuations on RES and demand.

#### 5.1.2 | Stability and stabilisation for time-delay ISGs

We consider the stability of time-delay ISGs embedded LFC in this subsection. Firstly, the global control input signal,  $u(t)$  can be rewritten in the form of  $u(t) = KCx(t)$  and the state space model of ISGs without FDIAs is

$$\dot{x}(t) = \bar{A}x(t) + \bar{A}_b x(t-b) + \Gamma d(t). \quad (41)$$

In system Equation (41),  $\bar{A}_b = \sum_{i=1}^N A_{bi}$ ,  $\bar{A} = A + BKC$  where  $A$ ,  $A_{bi}$ ,  $B$ ,  $\Gamma$  are defined in Equation (12). For ease of presentation, we consider  $b_i = b$  for all local SGs. We denote  $\tilde{x}(t) = \tilde{E}x(t)$ ,  $\tilde{x}(t) \in \mathbb{R}^n$ ,  $\tilde{E} \in \mathbb{R}^{n \times n}$  is the observation vector. This vector is for the evaluation of system robust performance,  $\gamma$ , presented in the relationship between the observation vector,  $\tilde{x}(t)$  and  $d(t)$  (the reader can refer to [20], [17] for the theory of robust stabilisation). For a given controller gain  $K$ , the following Theorem 3 presents a sufficient condition under which system Equation (41) is asymptotically stable with a pre-selected robust performance index (RPI),  $\gamma$ .

**Theorem 3.** For given positive scalars  $b, \gamma$ , and  $\tilde{\Lambda}$ , system Equation (41) is asymptotically stable with a given RPI,  $\gamma$ , if there exist symmetric positive definite matrices  $\tilde{P}, \tilde{Q}, \tilde{R} \in \mathbb{R}^{n \times n}$ , and  $\tilde{X} \in \mathbb{R}^{n \times n}$  satisfying the following matrix inequality

$$\tilde{\Lambda} = \begin{bmatrix} \tilde{\Lambda}_{11} & \tilde{\Lambda}_{12} & \tilde{\Lambda}_{13} \\ & \tilde{\Lambda}_{22} & 0 \\ & * & \tilde{\Lambda}_{33} \end{bmatrix} < 0, \quad (42)$$

where  $\tilde{\Lambda}_{11} = \sum_{j=0}^3 \Theta_j$ ,  $\tilde{\Lambda}_{12} = \mathcal{U}\Gamma$ ,  $\tilde{\Lambda}_{13} = \tilde{e}_0^T \tilde{E}^T$ ,  $\tilde{R} = b^2 \tilde{R}$ ,  $\Theta_0 = \tilde{e}_0^T \tilde{P} \tilde{e}_1 + \tilde{e}_1^T \tilde{P} \tilde{e}_0$ ,  $\tilde{R} = \text{diag}(\tilde{R}, \tilde{R}, \tilde{R})$ ,  $\tilde{\Lambda}_{22} = -\gamma^2 I_r$ ,  $\Theta_1 = \tilde{e}_0^T \tilde{Q} \tilde{e}_0 - \tilde{e}_2^T \tilde{Q} \tilde{e}_2 + \tilde{e}_1^T \tilde{R} \tilde{e}_1$ ,  $\Theta_2 = -\tilde{F}^T \tilde{R} \tilde{F}$ ,  $\tilde{\Lambda}_{33} = -I_v$ ,  $\Theta_3 = \mathcal{U}\mathcal{V} + \mathcal{V}^T \mathcal{U}^T$ ,  $\mathcal{U} = (\tilde{e}_0^T + \tilde{\lambda} \tilde{e}_1^T) \tilde{X}^T$ ,  $\tilde{\chi}(t) = [\mathbf{x}^T(t) \dot{\mathbf{x}}^T(t) \mathbf{x}^T(t-b) \tilde{\chi}_1^T(t) \tilde{\chi}_2^T(t)]^T$ ,  $\mathcal{V} = -\tilde{e}_1 + \tilde{A} \tilde{e}_0 + \tilde{A}_b \tilde{e}_2$ ,  $\tilde{\chi}_1(t) = \frac{1}{b} \int_{t-b}^t \mathbf{x}(s) ds$ ,  $\tilde{e}_l = [0_{(n) \times l(n)} \ I \ 0_{(n) \times (4-l)(n)}]$ ,  $0 \leq l \leq 4$ ,  $\tilde{F} = \begin{bmatrix} \tilde{e}_0 - \tilde{e}_2 \\ \tilde{e}_0 + \tilde{e}_2 - 2\tilde{e}_3 \\ \tilde{e}_0 - \tilde{e}_2 + 6\tilde{e}_3 - 6\tilde{e}_4 \end{bmatrix}$ ,  $\tilde{\chi}_2(t) = \frac{2}{b^2} \int_{t-b}^t \int_s^t \mathbf{x}(u) du ds$ .

*Proof of Theorem 3.* Let  $\tilde{P}, \tilde{Q}, \tilde{R}$  satisfy Equation (42). We construct the following Lyapunov–Krasovskii functional candidate  $\tilde{V}(\mathbf{x}(t), t) = \tilde{V}_1(t) + \tilde{V}_2(t) + \tilde{V}_3(t)$ ,  $\tilde{V}_1(t) = \mathbf{x}^T(t) \tilde{P} \mathbf{x}(t)$ ,  $\tilde{V}_2(t) = \int_{t-b}^t \mathbf{x}^T(s) \tilde{Q} \mathbf{x}(s) ds$ ,  $\tilde{V}_3(t) = b \int_{-b}^0 \int_{t+s}^t \dot{\mathbf{x}}(u) \tilde{R} \dot{\mathbf{x}}(u) du ds$ .

Then, we obtain  $\dot{\tilde{V}}(\mathbf{x}(t), t) = \tilde{\chi}^T(t) (\Theta_0 + \Theta_1) \tilde{\chi}(t) + J$ , where  $J = -b \int_{t-b}^t \dot{\mathbf{x}}(s) \tilde{R} \dot{\mathbf{x}}(s) ds$ . By using refined Jensen inequality,  $J \leq \tilde{\chi}^T(t) \Theta_2 \tilde{\chi}(t)$ . We use free-weighting matrix technique as follows  $\tilde{\chi}^T(t) \Theta_3 \tilde{\chi}(t) + \tilde{\chi}^T(t) \mathcal{U} \Gamma d(t) + d(t)^T \Gamma^T \mathcal{U}^T \tilde{\chi}(t) = 0$ .

Adding the left-hand side of the above equation to  $\dot{\tilde{V}}(t)$ , we have  $\dot{\tilde{V}}(\mathbf{x}(t), t) + \tilde{\chi}^T(t) \tilde{\xi}(t) - \gamma^2 d^T(t) d(t) \leq \tilde{\chi}_0^T(t) \tilde{\Lambda}_0 \tilde{\chi}(t)$ , where  $\tilde{\Lambda}_0 = \left\{ \begin{bmatrix} \tilde{\Lambda}_{11} & \tilde{\Lambda}_{12} \\ \tilde{\Lambda}_{12}^T & \tilde{\Lambda}_{22} \end{bmatrix} + \tilde{F}^T \tilde{F} \right\}$ ,  $\tilde{\chi}(t) = [\tilde{\chi}^T(t) \ d^T(t)]^T$  and  $\tilde{F} = [\tilde{E} \ 0]$ . By using Schur complement, the condition Equation (42) holds if and only if  $\Pi < 0$ . This leads to

$$\dot{\tilde{V}}(\mathbf{x}(t), t) + \tilde{\chi}^T(t) \tilde{\xi}(t) - \gamma^2 d^T(t) d(t) \leq 0. \quad (43)$$

Now, we are in the stage to prove that system Equation (41) is asymptotically stable with a RPI  $\gamma$ . For  $d(t) = 0$ , Equation (43) implies that  $\dot{\tilde{V}}(t)$  is negative definite, and thus system Equation (41) is asymptotically stable. For  $d(t) \neq 0$ , integrating both sides of Equation (43) from zero to  $t_f > 0$ , we obtain  $\tilde{V}(t_f) - \tilde{V}(0) + \int_0^{t_f} \tilde{\chi}^T(t) \tilde{\xi}(t) dt \leq \gamma^2 \int_0^{t_f} d^T(t) d(t) dt \leq \gamma^2 \int_0^\infty d^T(t) d(t) dt = \gamma^2 \|d\|^2$ . Therefore, if Equation (42) holds, the linear time-delay system with disturbance in Equation (41) will be asymptotically stable with a given RPI,  $\gamma$ . The proof of Theorem 3 is completed.  $\square$

As can be seen that, by using the above condition Equation (42), the stability of a closed-loop ISGs Equation (41) with pre-determined controller can be considered. This stability condition Equation (42) can be extended to cater for the design of a robust controller to stabilize ISGs asymptotically with a given RPI,  $\gamma$ .

### 5.1.3 | Stability of ISGs subjects to FDIAs

In this part, we will consider the stability of ISGs with FDIAs. Let we reform the state space model of ISGs from Equations (11) and (41) with the use of a static out feedback controller,

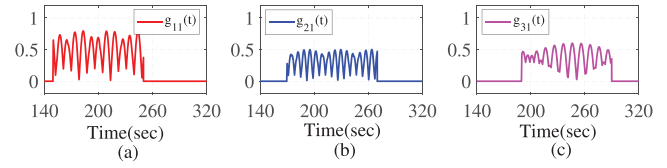


FIGURE 10 FDIAs on ACE: (a)  $g_{11}(t)$ , (b)  $g_{21}(t)$ , (c)  $g_{31}(t)$

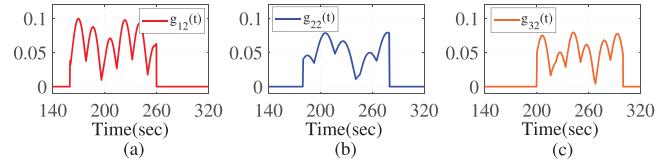


FIGURE 11 FDIAs on EVs: (a)  $g_{12}(t)$ , (b)  $g_{22}(t)$ , (c)  $g_{32}(t)$

$$u(t) = Ky(t).$$

$$\begin{aligned} \dot{\mathbf{x}}(t) &= \mathcal{A} \mathbf{x}(t) + \sum_{j=1, j \neq i}^N \mathcal{A}_{bi} \mathbf{x}(t - b_i) + \mathcal{S} g(t) + \Gamma d(t) \\ &\quad + BK(C \mathbf{x}(t) + F g(t)) \\ &= \bar{\mathcal{A}} \mathbf{x}(t) + \bar{\mathcal{A}}_b \mathbf{x}(t - b) + \Gamma_g d_g(t), \end{aligned} \quad (44)$$

where  $\Gamma_g = [\Gamma \ BKF + \mathcal{S}]$ ,  $d_g = [d^T \ g^T]^T$ . Note that  $d(t)$  includes REs fluctuation and  $g(t)$  is FDIAs vector.  $\bar{\mathcal{A}}, \bar{\mathcal{A}}_b$  is defined in Equation (41) for case  $b_i = b$ .

It can be observed that, for a given controller matrix gain  $K$ , matrices  $\mathcal{A}_g, \Gamma_g$  are known, system Equation (44) is presented in the form of a time-delay system with disturbance, which is similar to system Equation (41). Therefore, by applying the Theorem 3 for the system Equation (44) with known system matrices  $\bar{\mathcal{A}}, \bar{\mathcal{A}}_b$  and  $\Gamma_g$ , a stability of systems Equation (44) can be tested with a given RPI,  $\bar{\gamma}$ . It is noted that  $\bar{\gamma}$  represents the relationship between the observation vector,  $\tilde{\xi}(t)$  and  $d_g(t)$  which combines  $d(t)$  and  $g(t)$ .

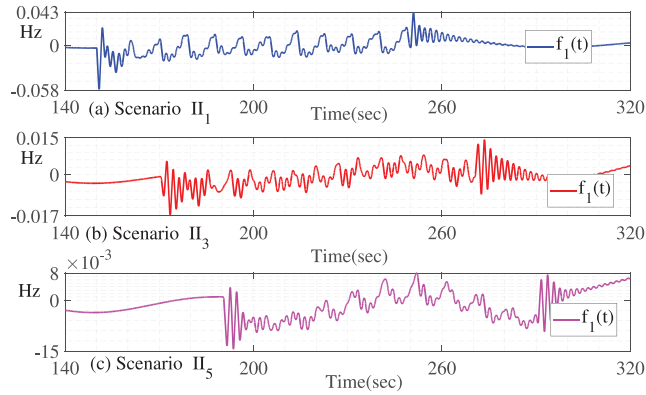
## 5.2 | Influences of FDIAs on LFC performance of ISGs

We take Scenario II of simulation to show the unfavourable impacts of FDIAs,  $g_{i1}(t), g_{i2}(t)$ ,  $i = 1, 2, 3$ , on the performance of closed-loop ISG. For demonstrative goal, FDIAs are considered as time-varying functions of  $g_{ij}(t) = a_{ij} |\sin(\sqrt{\delta_{ij}} t)| + \hat{a}_{ij} |(\cos \sqrt{\delta_{ij}} t)|$ , where  $a_{ij}, \hat{a}_{ij}, \sqrt{\delta_{ij}}, \sqrt{\delta_{ij}}$  are magnitudes and frequencies of sin and cos components. The FDIAs and their parameters are shown in Figures 10 and 11 and be tabulated in Table 1.

In this Scenario II, FDIAs happen in durations of 100 seconds for the six cases (Scenario II<sub>1</sub> to Scenario II<sub>6</sub>). The results of analysis are obtained by using MATLAB software version 2019b with the E15 Thinkpad Lenovo computer. The model of three-area ISGs is built by MALAB programming in m-file

**TABLE 1** FDIAs parameters in six case studies of Scenario II

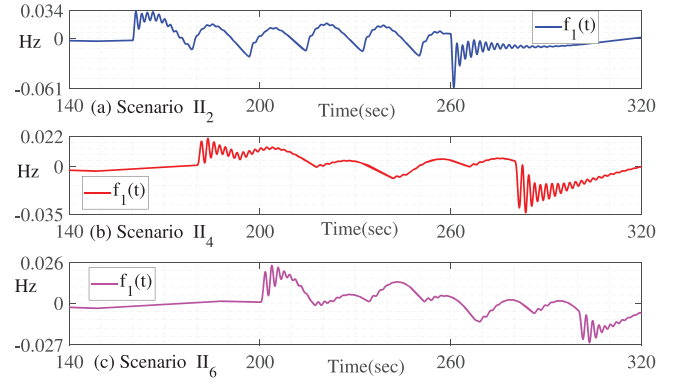
Scenario	$\Pi_1$	$\Pi_2$	$\Pi_3$	$\Pi_4$	$\Pi_5$	$\Pi_6$
	$g_{11}(t)$	$g_{12}(t)$	$g_{21}(t)$	$g_{22}(t)$	$g_{31}(t)$	$g_{32}(t)$
Start (s)	150	160	170	180	190	200
End (s)	250	260	270	280	290	300
$a_{ij}$	0.2	0.06	0.4	0.03	0.3	0.04
$\hat{a}_{ij}$	0.6	0.04	0.1	0.05	0.3	0.04
$\delta_{ij}$	0.07	0.031	0.21	0.017	0.09	0.005
$\hat{\delta}_{ij}$	0.13	0.003	0.3	0.002	0.11	0.033
FDIAs function: $g_{ij}(t) =  a_{ij} \sin(\sqrt{\delta_{ij}}t)  +  \hat{a}_{ij}(\cos \sqrt{\delta_{ij}}t) $						

**FIGURE 12** Abnormal responses of  $f_1(t)$  to  $g_1(t)$ : (a) Scenario  $\Pi_1$ , (b) Scenario  $\Pi_3$ , (c) Scenario  $\Pi_5$ 

which is convenient to observe the simulated signals for class of linear time-delay systems. The simulation step time is 0.01 s.

Figure 12 illustrates the responses of  $f_1(t)$  in abnormal operation of the ISG, where each FDIAs,  $g_{i1}(t)$ ,  $i = 1, 2, 3$  (FDIAs on computation of ACEs) are considered. It can be concluded that an individual FDIAs,  $g_{i1}(t)$  at a local power Area  $i^{\text{th}}$  can degrade not only the performance of local grid but also the neighbouring power areas. All three FDIAs,  $g_{i1}(t)$ ,  $i = 1, 2, 3$  on computation of  $ACE_i(t)$  (Scenarios  $\Pi_1$ ,  $\Pi_3$  and  $\Pi_5$ ) lead to unfavourable oscillations of  $f_1(t)$  during these times. Furthermore, after the FDIAs have left,  $f_1(t)$  was still oscillated from some seconds. By  $g_{11}(t)$ , the frequency deviation,  $f_1(t) \in [-0.058, 0.043]$  Hz, the deviation has increased ten to fourteen times compared to Scenario I where  $f_1(t) \in [-0.0062, 0.0039]$  Hz. For neighbouring power areas, the FDIAs of  $g_{21}(t)$ ,  $g_{31}(t)$  lead to the magnitude of fluctuation in frequency rises three times,  $f_1(t) \in [-0.011, 0.011]$  Hz, to six times,  $f_1(t) \in [-0.015, 0.08]$  Hz, than  $f_1(t)$  obtained in Scenario I (normal operation of the ISG).

Regarding to EVs, Figure 13 shows LFC performance of the closed-loop ISG in abnormal operations where each FDIAs,  $g_{i2}(t)$ ,  $i = 1, 2, 3$  (the FDIAs on aggregators of EVs) are considered. It can be seen from (Scenarios  $\Pi_2$ ,  $\Pi_4$  and  $\Pi_6$ ) that each FDIAs has made adverse impacts and leads to the low-quality in performance of  $f_1(t)$ . For example, in Scenario  $\Pi_2$ , the injection of  $g_{12}(t)$  FDIAs leads to  $f_1(t)$  fluctuates six times more than Scenario I. After the FDIAs finished, the frequency is still oscill-

**FIGURE 13** Abnormal responses of  $f_1(t)$  to  $g_2(t)$ : (a) Scenario  $\Pi_2$ , (b) Scenario  $\Pi_4$ , (c) Scenario  $\Pi_6$ 

lated. For FDIAs from neighbouring areas, the occurrence of  $g_{22}(t)$ ,  $g_{23}(t)$  FDIAs lead to the magnitudes of  $f_1(t)$  changes four to seven times than the result obtained in Scenario I. According to these simulations results, it is clear that the adverse impacts of FDIAs happened on both ACEs and aggregators of EVs are important and need to be considered for the efficient LFC operation of ISGs. In the next section of this paper, we will synthesize our proposed DFO based detectors to identify, isolate FDIAs. The co-operation of DFO detectors and isolators not only differentiate the FDIAs for between sub-systems but also differentiate FDIAs of ACE computations and EVs aggregators within a local SG.

### 5.3 | FDIAs detector synthesis

In this subsection, we are in the stage of synthesising the DFO detector gains,  $N_1$ ,  $N_{ib}$ ,  $J_i$ ,  $J_j$ ,  $H_i$ ,  $T_i$ ,  $E_i$  proposed in Sections 2–4. To do that, three local DOF detectors are designed and located at three local SGs to implement the task of detecting local FDIAs and triggering the alarm (or LED). The simulation data, time delays, RES fluctuations, and FDIAs are from Scenarios I-II.

We take Scenario III with the main focus on the design of local power Area-1<sup>st</sup>,  $\mathcal{D}_1$ . The main task of the detector,  $\mathcal{D}_1$ , is to detect the local FDIAs,  $g_{11}(t)$  and  $g_{12}(t)$ . The ultimate detective goals of  $\mathcal{D}_1$ , are explained as follows: (i) if the alarm/LED is ON, there is at least one FDIAs,  $g_{11}(t)$  or  $g_{12}(t)$ , happened; (ii) if the alarm/LED is OFF, there is no FDIAs of  $g_{11}(t)$  or  $g_{12}(t)$  happened at the power Area-1<sup>st</sup>. On the contrary, regarding to the existence of attacks: (iii) if any attacks of  $g_{11}(t)$  and  $g_{12}(t)$  happened, the LED is ON; iv) if no attack of  $g_{11}(t)$  and  $g_{12}(t)$  happened, the LED is OFF. System matrices  $\mathcal{A}_{11}$ ,  $\mathcal{A}_{11b}$ ,  $\mathcal{A}_{12}$ ,  $\mathcal{A}_{13}$ ,  $B_1$ ,  $C_1$ ,  $C_{12}$ ,  $C_{13}$ ,  $\Gamma_1$ ,  $F_{11}$ ,  $F_{12}$ ,  $S_{11}$ ,  $S_{12}$  are given in the Appendix. Time delay  $b_1 = 0.1$  s. There are six information comprising four local measurements and two remote signals required from remote power Areas 2<sup>st</sup> and 3<sup>rd</sup> are required for obtaining the gains of  $\mathcal{D}_1$ . By employing the synthesis procedure (Section 4), we obtained  $L_1$ ,  $J_{12}$ ,  $J_{13}$  in Step 1 and  $N_{11}$ ,  $N_{12}$ ,  $N_{1b1}$ ,  $N_{1b2}$ ,  $J_{101}$ ,  $J_{102}$ ,  $J_{1b1}$ ,  $J_{1b2}$  in Step 3 of the algorithm. All of these steps can be easily implemented by using Matlab



software with basic algebra. In Step 3, we solve Equation (38) to obtain  $Z_1$ , here (LMI) tool in Matlab robust control toolbox with an optimisation process containing searching parameter of  $\delta = 0.6$  are used. Accordingly,  $\mathbf{D}_1$ -detector's matrix gains,  $N_1$ ,  $N_{1b}$ ,  $J_1$ ,  $J_{1b}$ ,  $J_{12}$ ,  $J_{13}$  can be obtained as

$$N_1 = \begin{bmatrix} -1.113275 & 0 & 0 \\ 0 & -1.113275 & 0 \\ 0 & 0 & -1.113275 \end{bmatrix},$$

$$N_{1b} = \begin{bmatrix} -0.117131 & 0 & 0 \\ 0 & -0.117131 & 0 \\ 0 & 0 & -0.117131 \end{bmatrix}, H_1 = \begin{bmatrix} 0 \\ 0 \\ 0 \end{bmatrix},$$

$$J_1 = \begin{bmatrix} 0 & 0.113275 & 0 & 0 \\ 0.4905 & 0 & 1.113275 & 0 \\ 0.4250 & 0 & 1 & 1.113275 \\ 0 & 0 & 0 & 0 \end{bmatrix},$$

$$J_{1b} = \begin{bmatrix} -0.833333 & 0.117131 & 0 & 0 \\ 0 & 0 & 0.117131 & 0 \\ 0 & 0 & 0 & 0.117131 \end{bmatrix},$$

$$J_{12} = \begin{bmatrix} 0 \\ -0.2725 \\ 0 \end{bmatrix}, J_{13} = \begin{bmatrix} 0 \\ -0.2180 \\ 0 \end{bmatrix}.$$

As can be seen that  $N_1$  is three rows with full rank, therefore the order of the design DFO detector is third orders, which is smaller size than the order of FUO based detectors. We will discuss the advantage later. Now, we consider building the residual generator,  $r_1(t)$  for detector  $\mathbf{D}_1$ . The form of  $r_1(t)$  defined as  $r_1(t) = T_{1a}z_1(t) + E_{1a}y_1(t)$  from Equation (14), where  $z_1(t)$  is from the designed DFOs and pair matrices  $(T_1, E_1)$  can be obtained from Step 4 of the synthesis algorithm in Section 4. Theoretically,  $r(t) \neq 0$  is enough for the FDIAs detection. In practical implementation a comparable value,  $r_1^*(t) = |r_1(t)|$  should be developed and compared to a pre-determined values of system threshold  $\bar{r}_1(t)$  to trigger the alarm or turn on the LED. By employing Step 4 of the algorithm, we have found that there exist two values of residual generators,  $r_{1a}(t)$  and  $r_{1b}(t)$ , satisfying our conditions with two solution for pairs of  $(T_{1a}, E_{1a})$  and  $(T_{1b}, E_{1b})$ . Therefore, two residual values can be built as  $r_{1a}(t) = T_{1a}z_1(t) + E_{1a}y_1(t)$  and  $r_{1b}(t) = T_{1b}z_1(t) + E_{1b}y_1(t)$ .

However, by taking many tests, we recognised that the residual generators,  $r_{1a}(t)$  and  $r_{1b}(t)$ , may clearly reacts to one FDIAs but not strongly reacts to the other ones. In order to tackle the gap between the theoretical calculations and practical observations, we have taken the following consideration. To ensure the detector,  $\mathbf{D}_1$ , can detect all two FDIAs clearly, we develop the comparable value,  $r_1^*(t)$  as follows  $r_1^*(t) = \sqrt{(r_{1a}(t))^2 + (r_{1b}(t))^2}$  and undertake the comparison between  $r_1^*(t)$  and a threshold  $\bar{r}_1 = 10^{-l}$  to trigger the alarm. The schematic implementation of  $r^*(t)$  is shown in Figure 14.

Figure 15 presents  $r_1^*(t)$  and the alarm status when no attacks occurred to the local power Area 1<sup>st</sup>,  $g_{11}(t) = 0$  and  $g_{12}(t) = 0$ , (Scenario III<sub>1</sub>). As can be observed from Figure 15,  $r_1^*(t) = 0$

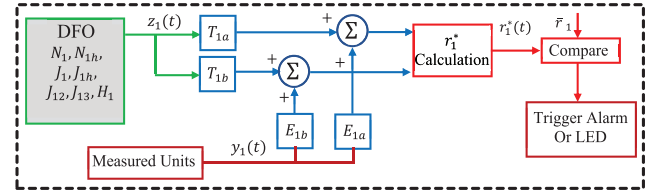


FIGURE 14 Schematic implementation of  $r_1^*(t)$

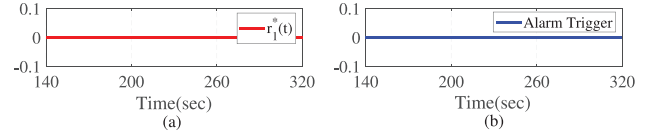


FIGURE 15 Detector responses when no FDIAs in the system (Scenario III<sub>1</sub>): (a)  $r_1^*(t)$ , (b) Triggered alarm status

and the Alarm (LED) is “OFF” with status “0”. On the other hand, Figures 16 and 17 illustrate  $r_1^*(t)$  and Alarm status when each attack,  $g_{11}(t)$  and  $g_{12}(t)$ , happened at the local power Area 1<sup>st</sup> (Scenarios III<sub>2</sub> to III<sub>3</sub>). As can be seen from Figures 16 and 17, when  $r_1^*(t)$  is clearly larger than threshold, the proposed detector can recognize  $g_{11}(t)$ ,  $g_{12}(t)$  clearly. Regarding to the alarm status, the alarm is triggered to On (set to be 1) in Scenarios III<sub>2</sub> to III<sub>3</sub>. For example,  $g_{11}(t) \neq 0$  in scenario III<sub>2</sub>, the alarm/LED is zero before the attack happened and triggered during 150 to 250 s period. These results also indicate that after the FDIAs has left, the alarm status go back to zeros after some seconds of settling time.

## 5.4 | FDIAs isolation scheme

The isolation of each local FDIA positions in the local power areas is also very important. The information of each local FDIA position is used to improve monitoring activities of local power grids (further action to handle the attacks). By using

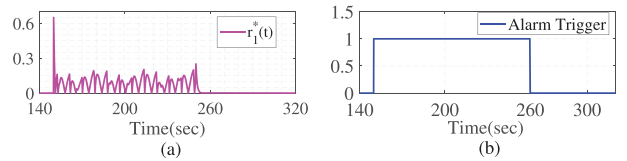


FIGURE 16 DFO detector responses to  $g_{11}(t)$  (Scenario III<sub>2</sub>): (a)  $r_1^*(t)$ , (b) Triggered alarm status

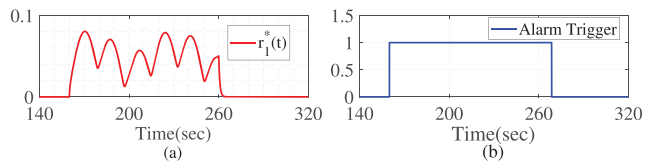
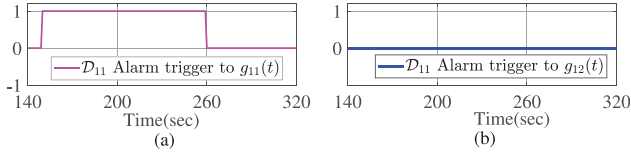


FIGURE 17 DFO detector responses to  $g_{12}(t)$  (Scenario III<sub>3</sub>): (a)  $r_1^*(t)$ , (b) Triggered alarm status

**TABLE 2** Isolating each local FDIAs,  $g_{11}(t)$  and  $g_{12}(t)$ 

Local attacks	Detector $\mathcal{D}_1$	Detector $\mathcal{D}_{11}$	Detector $\mathcal{D}_{12}$
No FDIA	OFF	OFF	OFF
$g_{12}(t)$	ON	OFF	ON
$g_{11}(t)$	ON	ON	OFF

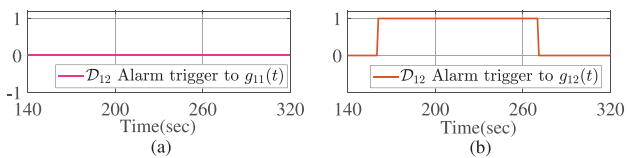
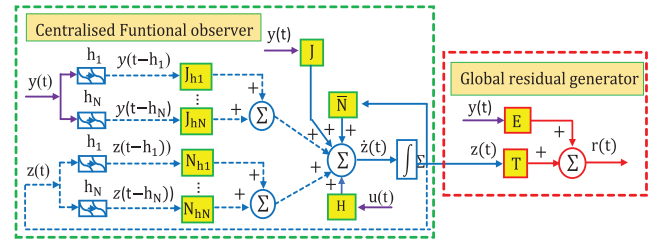
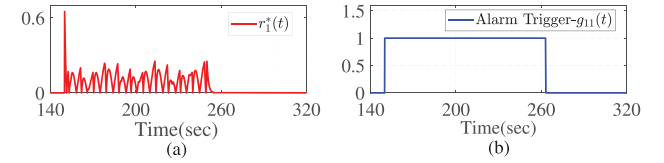
**FIGURE 18**  $\mathcal{D}_{11}$  responses to FDIAs: (a)  $g_{11}(t)$ , (b)  $g_{12}(t)$ 

distributed detection methods, each local detector can realise the existence of local FDIA at local power areas and the FDIA in other power Areas do not impact to the performance of the local detector. It implies that the local FDIA is isolated to others from neighbouring areas. In this part, we further to isolate each local FDIAs at a local power area. This means the isolators differentiates the existences of  $g_{11}(t)$  and  $g_{12}(t)$ . The main concept bases on the design the detector (residual generator-based observer) that insensitively reacts to one FDIA and sensitively reacts the remaining of FDIA. To do that, we develop two more local detectors: (i)  $\mathcal{D}_{11}$  is insensitive to  $g_{12}(t)$  and sensitive to  $g_{11}(t)$ ; (ii)  $\mathcal{D}_{12}$  is insensitive to  $g_{11}(t)$  and sensitive to  $g_{12}(t)$ . By using detectors,  $\mathcal{D}_1$ ,  $\mathcal{D}_{11}$  and  $\mathcal{D}_{12}$ , the isolation of two local FDIAs is obtained (see Table 2).

In order to show the effectiveness of the proposed isolation schemes, we undertook the Scenario IV. At first, by using apply Remark 3 and detector design in Section 3, the two second order DFO based detectors,  $\mathcal{D}_{11}$ ,  $\mathcal{D}_{12}$  are obtained to recognize each local individual FID,  $g_{11}(t)$  and  $g_{12}(t)$ . Figures 18 and 19 show the Alarm status of each detector to the existence of local FDIAs,  $g_{11}(t)$ ,  $g_{12}(t)$ . As can be seen that, the  $\mathcal{D}_{11}$  is insensitive to  $g_{11}(t)$  while it reacts to  $g_{12}(t)$  clearly. It is an important objective of our paper.

## 5.5 | Advantages of DFO scheme

As we have discussed in the introduction, the adverse impacts of REs intermittent need to be eliminated in the design of detectors. In Theorem 1 (see Equations (16) and (17)), the constraint of  $\Omega_{i1} = 0$  has been added to ensure that the variation in high frequency of REs will not impact the performance of detector.

**FIGURE 19**  $\mathcal{D}_{12}$  responses to FDIAs: (a)  $g_{11}(t)$ , (b)  $g_{12}(t)$ **FIGURE 20** Schematic implementation of the CFO based detector**FIGURE 21** CFO Detector responses to  $g_{11}(t)$  (Scenario V): (a)  $r_1^*(t)$ , (b) triggered alarm status

Indeed, the above section of detector synthesis has shown that advantage. By employing the constraint of  $\Omega_{j5}$ ,  $\Omega_{j6}$  to guarantee that the neighbouring FDIAs does not convert into the residual of generator, therefore, it is clear that our DFO detector is insensitive to those remote FDIAs. On the other hand, our proposed DFOs detector scheme is a distributed architecture and having advantage of minimum orders which are the main presentation in this subsection.

### 5.5.1 | Distributed implementation

The main characteristic of our proposed scheme is a distributed structure. By this, a detector of low order is located at each area of a SG to detect the local FDIAs only rather than to detect all FIDAs within the global power grid based on a centralised detector leading to the convenience of easy implementation. To verify that, in this subsection, we consider CFO based detector to recognise all FDIAs within SGs. According to the Remark 3 in Section 2 and a procedure which is similar to Section 4, a sixth-order CFO detector can be obtained. The schematic of implementation of CFOs detector are given in Figure 20.

Clearly, CFO detector requires the access of large number of instant information of control signals and measurements contemporarily. In contrast, the proposed DFO detector needs less information so that less cost of implementation. Furthermore, CFO detector requires a large central facility which can be sensitive to malicious incidents. Similar to the processing of building comparable value for DFO detector, to avoid some sensitivities of practical calculation, the global centralised comparable value of  $r^*$  is computed based on six residual generators,  $r^* = \sqrt{\sum_{j=1}^6 (r_j(t))^2}$ . Figures 21 and 22 (Scenario V) show the performance of the CFO detector. As can be seen that, the CFO detector can implement the task of detecting FDIAs,  $g_{11}(t)$  and  $g_{12}(t)$ . However, it is noted that, it has disadvantage as we have discussed above.

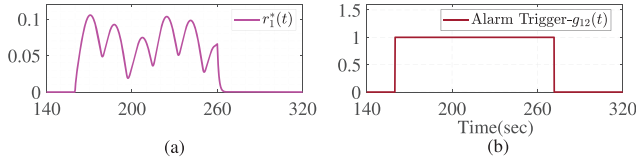


**FIGURE 22** CFO detector responses to  $g_{11}(t)$  (Scenario V): (a)  $r_1^*(t)$ , (b) triggered alarm status

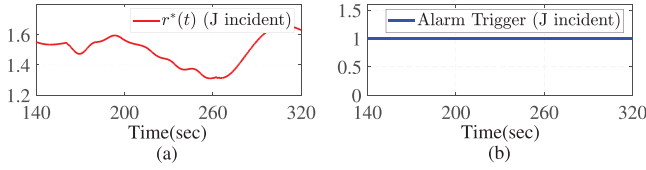


**FIGURE 23** CFO Detector responses to  $g_{12}(t)$  in (J-incident): (a)  $r^*(t)$ , (b) triggered alarm status

In the following part, we conduct Scenario VI to consider the situation that the centralised facility of CFO detector is impacted by malicious incidents. For example, CFO detector's gains of  $N, J$ , are destroyed and considered as null matrix from the seconds of 100 to 400. It is noted that the whole ISGs now have only one detector. The performance of CFO detector under malicious incidents of  $N$  and  $J$  are respectively shown in Figures 23 and 24. From these results of Scenario VI, it is clear that when the central facility of the CFOs detector operates under the abnormal of malicious incidents, the performance of detector is degraded or further destroyed leading to the incorrect activities in implementing the task of detecting  $g_{12}(t)$ , i.e. the alarm operates incorrectly.

### 5.5.2 | Minimum-order detector

Another advantage of our detection scheme is that our detector is reduced order (small size and weigh). The order of our DFO detector is determined according to the number of independent rows of  $L_i$ , further, the rank of matrix  $N_i$ . Therefore, to minimize the size of detector, number of rows of matrix  $L_i$  should be minimized. This purpose can be achieved by considering Step 1 of the procedure. In this step,  $L_i$  is selected to satisfy the condition Equation (34) as  $\Psi_i \Xi_i = 0$ , where  $\Psi_i$  contains  $L_i$  as  $\Psi_i = [\Xi_{ic} \ L_i]$ , and  $\Xi_{ic}$  are given in Step 1. In previous section, by obtaining  $\Psi_i$  and further  $L_i$  has three rows and third-order DFO detector is designed. By minimizing the number of rows of  $\Psi_i$ , a second-order DFO detector can be obtained. There-

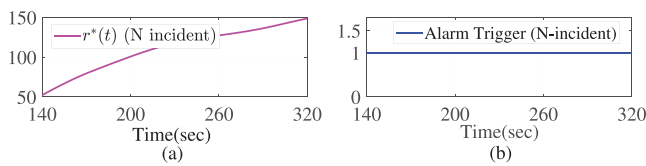


**FIGURE 24** CFO Detector responses to  $g_{12}(t)$  in (N-incident): (a)  $r^*(t)$ , (b) triggered alarm status

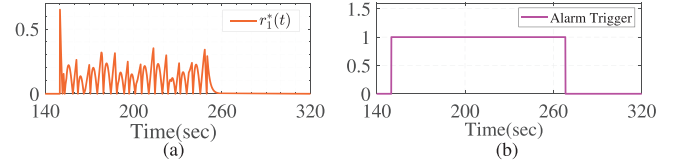


**FIGURE 25** CFUO detector responses to  $g_{11}(t)$  (Scenario VII): (a)  $r_1^*(t)$ , (b) triggered alarm status

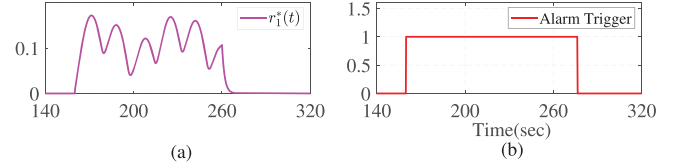


**FIGURE 26** CFUO detector responses to  $g_{12}(t)$  (Scenario VII): (a)  $r_1^*(t)$ , (b) triggered alarm status

fore, our detection method can achieve a very small size of the detector. This is the important motivation behind our research.

In order to further highlight the advantages of FOs, we use full-order state observer to design CFUO detector and compare to the CFO detector. The structure of unknown input CFUO has been extensively considered in [30] and the CFUO detector can be designed from chapter 2 in [30] and our procedure in Section 4. Here, the CFUO comparable signal is built as  $r^*(t) = |y(t) - C\hat{x}(t)|$  where  $\hat{x}(t)$  is the estimation of the state vector  $x(t)$ . For a three-area ISG, the order of CFUO based detector is always equal to the number of the state variables which is 20. This order is significantly higher than sixth-order of CFO detector (presented in Section 5.5.1) and third-order DFO detector (presented in Section 5.3) and second-order DFO detector (in above discussion). Figures 25 and 26 show the performance of CFUO based detector subjects to FDIAs,  $g_{11}(t)$ ,  $g_{12}(t)$ . As can be seen that, the observer can implement the task of detecting FDIAs, however, as we have presented, the order of this observer is significant high leading to high cost of computation.

With regard to eigenvalue, let we consider ISGs without time-delay and the DFOs detector for Area-1<sup>st</sup> is

$$\begin{aligned} r_1(t) &= T_1 \tilde{z}_1(t) + E_1 y_1(t), \\ \dot{\tilde{z}}_1(t) &= N_1 \tilde{z}_1(t) + J_1 y_1(t) + H_1 u_1(t) + J_{12} \tilde{y}_2(t) + J_{13} \tilde{y}_3(t), \end{aligned} \quad (45)$$

where  $N_1, J_1, J_{12}, J_{13}, T_1, E_1$  are detectors' gains. It is noted that  $N_{1b}, J_{1b}$  are not considered due to the invalid of time-delay. By using similar technique in Section 3, a DFOs based detector without time-delay consideration can be obtained (we call it as  $\tilde{D}_1$ ). Without FDIAs consideration, the observer error is  $\tilde{\theta}_1(t) = N_1 \theta_1(t)$ . Now we combine state space model of original IGSS with DFOs as follows

$$\begin{aligned} \begin{bmatrix} \dot{x}(t) \\ \dot{\theta}_1(t) \end{bmatrix} &= \begin{bmatrix} \tilde{A} & 0 \\ 0 & N_1 \end{bmatrix} \begin{bmatrix} x(t) \\ \theta_1(t) \end{bmatrix} + \begin{bmatrix} \Gamma \\ 0 \end{bmatrix} d(t) \\ &= A_N x_N(t) + \Gamma_N d(t). \end{aligned} \quad (46)$$

where  $\tilde{A} = \bar{A} + \bar{A}_b$ .  $\bar{A}$  and  $\bar{A}_b$  are defined in Equation (44).

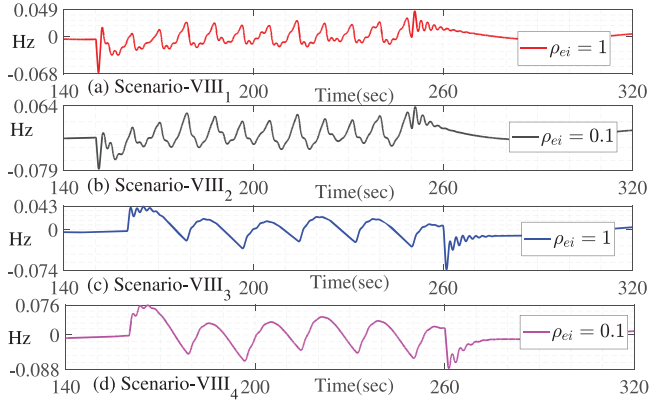


FIGURE 27 Responses of  $f_1(t)$  under FIDAs for different  $\rho_{ei}$

As can be seen that the eigenvalues  $\mathcal{A}_N = \begin{bmatrix} \tilde{\mathcal{A}} & 0 \\ 0 & N_1 \end{bmatrix}$  combines the eigenvalues of  $\tilde{\mathcal{A}}$  and eigenvalues of  $N_1$ . By using eig function in MATLAB, we obtain the similar results.

## 5.6 | EVs frequency support analysis

In this part, we undertake an analysis on the contribution of EVs to the frequency regulation. In this paper, EVs participate into LFC via the operation of droop loop which mimics the operation of power plant's primary frequency regulation. The contribution of EVs into the frequency service is presented by EVs droop constant  $\rho_{ei}$ . Throughout of all previous parts,  $\rho_{ei} = \hat{\rho}_{ei}/R_{gi}$ , where  $\hat{\rho}_{ei} = 2$ , hence EVs contribute  $\frac{\rho_{ei}}{(\rho_{ei}+1/R_{gi})} = 67\%$  into the services. Under the impacts of FDIAs  $g_{11}(t)$  and  $g_{12}(t)$ , the system frequency,  $f_1(t)$  belongs to the range of  $[-0.058 \text{ Hz}; 0.043 \text{ Hz}]$  and  $[-0.061 \text{ Hz}; 0.034 \text{ Hz}]$  respectively. By employing the stability condition presented in subsection 5.1, the maximum value of  $\rho_{ei}$  while the system still be stable is around  $3/R_{gi}$ , which presents 75% of frequency service.

To emphasis on the effect of EVs contribution in abnormal operation of FDIAs, we observe the systems performance under abnormal operations subjects to  $g_{11}(t)$  and  $g_{12}(t)$  when  $\hat{\rho}_{ei}$  changes. By adjusting the values of  $\hat{\rho}_{ei}$  from 0.1 to 1, the contribution of EVs is from 9% to 50%. Figure 27 shows the responses of  $f_1(t)$  in some abnormal operations. As can be seen that, under the impacts of FIDAs, for  $\rho_{ei}$  smaller than  $3/R_{gi}$ , better performance of  $f_1(t)$  can be achieved with more contributions of EVs.

For the case of  $g_{11}(t) \neq 0$ , (iii) (Scenario VIII<sub>1</sub>):  $f_1(t) \in [-0.068; 0.049] \text{ Hz}$  EVs contributes 50% of the service, iv) (Scenario VIII<sub>2</sub>):  $f_1(t) \in [-0.079; 0.064] \text{ Hz}$  while EVs contributes 9%. On the other hand, for the case of  $g_{12}(t) \neq 0$ , (i) (Scenario VIII<sub>3</sub>):  $f_1(t) \in [-0.074; 0.043] \text{ Hz}$  while EVs contributes 50% of the service, (ii) (Scenario VIII<sub>4</sub>):  $f_1(t) \in [-0.088; 0.076] \text{ Hz}$  while EVs contributes 9%.

In summary, with extensive analysis and evaluation through Section 5, we have demonstrated the capability of our proposed DFO based detection scheme.

## 6 | CONCLUSION

In this paper, the issue of FDIAs on LFC of ISGs has been considered. A new mathematic representation of ISGs incorporated FDIAs, intermittent of RES, aggregated EVs with communication delays has been proposed. With the goal of detecting and isolating FDIAs within ISG, we have derived a new DFO based detection and isolation schemes based on some developments of FOs, stability of time-delay systems, EVs integrations and residual generator-based fault detection. We have proposed an effective procedure in tractable LMIs and an optimisation process for synthesising the detector's gains. This procedure can be easily solved by robust control toolbox in MATLAB with together with C Programming. Our DFOs detectors have the advantages of insensitive to neighbouring FDIAs and REs variation, malicious incident of centralised architecture while being able to deal with time delays. Furthermore, the detector has smaller size than the conventional state observer-based detectors. The distributed architecture of detector leads to the reduction in cost of computation and the convenience for implementation monitoring tasks. We have also discussed the stability of time-delay ISGs and the EVs contributions into frequency service under abnormal of FDIAs. Various comprehensive simulations have been carried out with a three-area ISG to validate the effectiveness of the proposed scheme. The studied SGs can be enlarged to include various topologies of ISGs. In the future work, the design method of this paper can be extended to deal with wider classes of systems that include non-linearities. On the other hand, the stabilisation and mitigation problem for ISGs should be further addressed. In this case, the combination of DFOs and decentralised controller needs further development.

## NOMENCLATURE

EVs, LFC	Electric vehicles, load frequency control.
ISG, RES	Interconnected smart grid, renewable energies.
FDIA, FDO	False data injection attack, full-order observer.
DFO, CFO	Distributed and centralised functional observer.
LMI	Linear matrix inequality.
LKF	Lyapunov Krasovskii functionals.
$i, b_i$	Power Area- $i^{th}$ , time delay.
$\delta_i, \tilde{\delta}$	Optimisation searching variables in LMI.
$n_i$	The number of state variables of Area- $i^{th}$ .
$M_i, D_i$	Inertia constant, load damping coefficient.
$f_i, b_i$	Frequency deviation, frequency bias constant.
$R_{gi}, \rho_{ei}$	Governor and EVs droop characteristic.
$K_{gi}, K_{ti}$	Governor and turbine gain constants.
$K_{ei}, T_{ei}$	EVs gain and time constants.
$T_{gi}, T_{ti}$	Governor and turbine time constants.
$K_{ri}, T_{ri}$	Reheater gain and time constants.
$ACE_i, b_i$	Area control error, frequency bias constant.
$P_{li}, P_{wi}$	Load demand and wind power deviations.
$X_{gi}, P_{ei}$	Governor position and EVs power deviations.
$P_{gi}, P_{ri}$	Power and reheater output deviations.



$P_{ci}$	Incremental change in power command.
$g_{i1}, g_{i2}$	FDIAs at power plants and aggregators.
$g_{emi}$	FDIA at aggregator related to the $m^{th}$ EV.
$\theta_i$	Integral value of area error control.
$r_i(t), r_i^*(t)$	Residual generator and detector comparable value.
	$N_i, N_{ib}, J_i, J_{ij}, H_i, J_{ib}, L_i$ and $T_i, E_i$ are detector's matrices.

## ORCID

Thanh Ngoc Pham  <https://orcid.org/0000-0002-1055-2875>

Hieu Trinh  <https://orcid.org/0000-0003-3438-9969>

## REFERENCES

- Kundur, P.: Power system stability and control. McGraw-Hill, New York, NY (1994).
- Ibraheem, et al.: Recent philosophies of automatic generation control strategies in power systems. *IEEE Trans Power Syst.* 20(1), 346–357 (2005)
- Pham, T. N., et al.: Load frequency control of power systems with electric vehicles and diverse transmission links using distributed functional observers. *IEEE Trans. Smart Grid* 7(1), 238–252 (2016)
- Sun, C. C., et al.: Cyber security of a power grid: state-of-the-art. *Int. J. Elect. Power Energy Syst.* 99, 45–56 (2018)
- Wang, W., Lu, Z.: Cyber security in the smart grid: survey and challenges. *Comput. Networks* 57(5), 1344–1371 (2013)
- Ding, D., et al.: A survey on security control and attack detection for industrial cyber-physical systems. *Neurocomputing* 275, 1674–1683 (2018)
- Wang, Q., et al.: Review of the false data injection attack against the cyber-physical power system. *IET Cyber-Physical Syst. Theory Appl* 4(2), 101–107 (2019)
- Ten, C. W., et al.: Vulnerability assessment of cyber security for SCADA systems. *IEEE Trans. Power Syst.* 23(4), 1836–1846 (2008)
- Johnson, J., et al.: Power system effects and mitigation recommendations for DER cyber attacks. *IET Cyber-Physical Syst. Theory Appl.* no. 3 4(3), 240–249 (2019)
- Afshari, A., et al.: Resilient synchronization of voltage/frequency in AC microgrids under deception attacks. *IEEE Syst. J.* (2020). <https://doi.org/10.1109/JSYST.2020.2992309>
- Sargolzaei, A., et al.: Resilient design of networked control systems under time delay switch attacks, application in smart grid. *IEEE Access* 5, 15901–15912 (2017)
- Peng, C., et al.: Resilient event-triggering  $H_\infty$  load frequency control for multi-area power systems with energy-limited DoS attacks. *IEEE Trans. Power Syst.* 32(5), 4110–4118 (2017)
- Tan, R., et al.: Modeling and mitigating impact of false data injection attacks on automatic generation control. *IEEE Trans. Inf. Forensics Secur.* 12(7), 1609–1624 (2017)
- Chen, C., et al.: Novel detection scheme design considering cyber attacks on load frequency control. *IEEE Trans. Ind. Informat.* 14(5), 1932–1941 (2018)
- Sridhar, S., Govindarasu, M.: Model-based attack detection and mitigation for automatic generation control. *IEEE Trans. Smart Grid* 5(2), 580–591 (2014)
- Huang, T., et al.: An online detection framework for cyber attacks on automatic generation control. *IEEE Trans. Power Syst.* 33(6), 6816–6827 (2018)
- Pham, T. N., et al.: Static output feedback frequency stabilization of time-delay power systems with coordinated electric vehicles state of charge control. *IEEE Trans. Power Syst.* 32(5), 3862–3874 (2017)
- Pham, T. N., et al.: Distributed control of HVDC links for primary frequency control of time-delay power systems. *IEEE Trans Power Syst* 34(2), 1301–1314 (2019)
- Pham, T. N., et al.: Decentralized bounded input bounded output stabilization of perturbed interconnected time-delay power systems with energy storages. *Int. J. Elect. Power Energy Syst.* 93, 51–64 (2017)
- Pham, T. N., et al.: Integration of electric vehicles for load frequency output feedback  $H_\infty$  control of smart grids. *IET Gener., Transm., Distrib.* 10(13), 3341–3352 (2016)
- Baghaee, H. R., et al.: A generalized descriptor-system robust  $H_\infty$  control of autonomous microgrids to improve small and large signal stability considering communication delays and load nonlinearities. *Int. J. Elect. Power Energy Syst.* 92, 63–82 (2017)
- Borojeni, K. G., et al.: Smart grids: security and privacy issues. Springer, Berlin (2017)
- Habibi, M. R., et al.: Detection of false data injection cyber-attacks in DC microgrids based on recurrent neural networks. *IEEE J. Emerging Select. Power Electr.* (2020). <https://doi.org/10.1109/JESTPE.2020.2968243>
- Luo, X., et al.: Detection and isolation of false data injection attack for smart grids via unknown input observers. *IET Gener., Transm., Distrib.* 13(8), 1277–1286 (2019)
- Aldeen, M., Sharma, R.: Robust detection of faults in frequency control loops. *IEEE Trans Power Syst* 22(1), 413–422 (2007)
- Ameli, A., et al.: Attack detection and identification for automatic generation control systems. *IEEE Trans. Power Syst.* 33(5), 4760–4774 (2018)
- Ameli, A., et al.: Attack detection for load frequency control systems using stochastic unknown input estimators. *IEEE Trans. Inf. Forensics. Secur.* 13(10), 2575–2590 (2018)
- Caliskan, F., Genc, I.: A robust fault detection and isolation method in load frequency control loops. *IEEE Trans Power. Syst.* 23(4), 1756–1767 (2008)
- Alhelou, H. H., et al.: Robust sensor fault detection and isolation scheme for interconnected smart power systems in presence of RER and EVs using unknown input observer. *Int. J. Elect. Power Energy Syst.* 99, 682–694 (2018)
- Trinh, H., Fernando, T.: Functional observers for dynamical systems. Springer-Verlag, Berlin (2012)
- Teh, P. S., Trinh, H.: Design of unknown input functional observers for nonlinear systems with application to fault diagnosis. *J. Process Contr.* 23(8), 1169–1184 (2013)
- Yang, T. Y., et al.: Functional observer design for time-delayed systems with application to fault diagnosis. *IEEE Access* 7, 14558–14568 (2019)
- Tran, H. M., Trinh, H.: Distributed functional observer based fault detection for interconnected time-delay systems. *IEEE Syst. J.* 13(1), 940–951 (2019)
- Rao, C. R., Mitra, S. K.: Generalized Inverse of Matrices and Its Applications. Wiley, Weinheim (1971)
- Hien, L. V., Trinh, H.: Refined Jensen based inequality approach to stability analysis of time delay systems. *IET Control Theory Appl.* 9(14), 2188–2194 (2015)

**How to cite this article:** Pham TN, Oo AT, Trinh H. Detecting and isolating false data injection attacks on electric vehicles of smart grids using distributed functional observers. *IET Gener Transm Distrib.* 2020;1–18. <https://doi.org/10.1049/gtd2.12057>

## APPENDIX A

Simulation data of the ISG in Figure 1 is given [1, 3 17] as follows:

$$K_{ti} = 1, T_{ti} = 0.3, K_{gi} = 1, T_{gi} = 0.08, R_{gi} = 2.4,$$

$$K_{ri} = 5, T_{ri} = 10, M_i = 0.1667, b_i = 0.425, D_i = 0.0083,$$

$$T_{ei} = 1, K_{ei} = 1, \rho_{ei} = 2/R_{gi}, 2\pi T_{12} = 0.2725,$$

$$2\pi T_{13} = 0.2180, 2\pi T_{23} = 0.1635, T_{ji} = T_{ij}, i = 1, 2, 3.$$

Matrices  $A_{ii}, A_{iib} \in \mathbb{R}^{n_i \times n_i}, A_{ij} \in \mathbb{R}^{n_i \times n_j}, C_i \in \mathbb{R}^{p_i \times n_i}, B_i, \Gamma_i, S_{i1}, S_{i2} \in \mathbb{R}^{n_i \times 1}, F_{i1}, F_{i2} \in \mathbb{R}^{p_i \times 1}$ , are

$$A_{ii} = \begin{bmatrix} \frac{-D_i}{M_i} & 0 & 0 & \frac{1}{M_i} & \frac{1}{M_i} & \frac{-1}{M_i} & 0 \\ \frac{-1}{R_{gi}T_{gi}} & \frac{-1}{T_{gi}} & 0 & 0 & 0 & 0 & 0 \\ 0 & \frac{K_{ii}}{T_{ii}} & \frac{-1}{T_{ii}} & 0 & 0 & 0 & 0 \\ 0 & \frac{K_{ri}K_{ii}}{T_{ii}T_{ri}} & \frac{T_{ii}-K_{ri}}{T_{ii}T_{ri}} & \frac{-1}{T_{ri}} & 0 & 0 & 0 \\ 0 & 0 & 0 & 0 & \frac{-1}{T_{ei}} & 0 & 0 \\ \beta_{i1} & 0 & 0 & 0 & 0 & 0 & 0 \\ b_i & 0 & 0 & 0 & 0 & 1 & 0 \end{bmatrix},$$

$$A_{ij} = \begin{bmatrix} 0_{5 \times 1} & 0_{5 \times (n_j-1)} \\ -2\pi T_{ij} & 0_{1 \times (n_j-1)} \\ 0 & 0_{1 \times (n_j-1)} \end{bmatrix}, A_{iib} = \begin{bmatrix} 0_{4 \times 1} & 0_{4 \times (n_i-1)} \\ \frac{-K_{ii}\rho_{ei}}{T_{ei}} & 0_{1 \times (n_i-1)} \\ 0_{2 \times 1} & 0_{2 \times (n_i-1)} \end{bmatrix},$$

$$B_i = \begin{bmatrix} 0 \\ \frac{K_{gi}}{T_{gi}} \\ 0_{(n_i-2) \times 1} \end{bmatrix}, \Gamma_i = \begin{bmatrix} \frac{-1}{M_i} \\ 0_{(n_i-1) \times 1} \end{bmatrix}, S_{i2} = \begin{bmatrix} 0_{4 \times 1} \\ \frac{K_{ii}}{T_{ii}} \\ 0_{(n_i-5) \times 1} \end{bmatrix},$$

$$S_{i1} = [0_{n_i \times 1}], F_{i2} = [0_{p_i \times 1}], \beta_{i1} = 2\pi \sum_{j=1, j \neq i}^N T_{ij}.$$

$$C_i = \begin{bmatrix} 1 & 0_{1 \times (n_i-3)} & 0 & 0 & 0 \\ 0 & 0_{1 \times (n_i-3)} & 1 & 0 & 0 \\ 0 & 0_{1 \times (n_i-3)} & 0 & 1 & 0 \\ 0 & 0_{1 \times (n_i-3)} & 0 & 0 & 1 \end{bmatrix}, F_{i1} = \begin{bmatrix} 0_{(p_i-1) \times 1} \\ 1 \end{bmatrix}.$$

For the design of  $\mathcal{D}_1$ ,  $C_{ij} = [1 \ 0_{1 \times (n_j-1)}]$ ,  $\bar{F}_{ij} = [0_{1 \times 2}]$ ,  $E_{1a} = [0 \ 1 \ 0 \ 0]$ ,  $E_{1b} = [0 \ 0 \ 0 \ 1]$ ,  $T_{1a} = [-1 \ 0 \ 0]$ ,  $T_{1b} = [0 \ 0 \ -1]$ .